European Journal of Medicinal Chemistry 247 (2023) 115073

Contents lists available at ScienceDirect

European Journal of Medicinal Chemistry

journal homepage: www.elsevier.com/locate/ejmech

Research paper

Real-time detection of T cell activation by visualizing TCR nanoclusters with a cholesterol derived aggregation-induced emission probe

Kaiming Li [a,b,1], Yue Chen [a,1], Nianci Zhu [a,b], Sijia Chen [a,b], Meng Jia [c], Lingjing Xue [a,b], Meixi Hao [a,b,**], Can Zhang [a,b,*]

[a] State Key Laboratory of Natural Medicines, Jiangsu Key Laboratory of Drug Discovery for Metabolic Diseases, Jiangsu Key Laboratory of Drug Design and Optimization, Center of Advanced Pharmaceuticals and Biomaterials, China Pharmaceutical University, Nanjing, 210009, China
[b] Chongqing Innovation Institute of China Pharmaceutical University, Chongqing, 401135, China
[c] Nanjing University, School of Life Sciences, Nanjing, 210093, China

ARTICLE INFO

Handling Editor: Dr. Z Liu

Keywords:
TCR nanoclusters visualization
T cell activation
Cholesterol derived probe
Aggregation-induced emission

ABSTRACT

Successful T-cell based immunotherapy usually depends on the activation of T cells. Most of commonly used methods for assessing T cell activity rely on the antibody-based technology, which focus on detecting protein-centered activation markers, including CD25, cytokines and so on. However, these methods always involve tedious sample-preparation process, labor-consuming and costly, which could not be utilized in real-time detection. The T cell receptor (TCR) clustering is another kind of essential T cell activation marker on the membrane, which increases during the activation state of T cells. We herein developed a cholesterol derived aggregation-induced emission (AIE) fluorescent probe (R-TPE-PEG-Chol) for detecting T cell activation in real-time. Five probes were first designed and synthesized and among them COOH-TPE-PEG-Chol displayed the best imaging effects, which had no significant impact on the key physiological functions of T cells. In addition, we have proved that COOH-TPE-PEG-Chol was introduced onto the naïve T cell membrane in its molecularly dissolved form without fluorescent emission. While during T cell activation, the formation of TCR nanoclusters would induce aggregation of membrane cholesterol, which could provoke the fluorescence signal of the COOH-TPE-PEG-Chol due to the AIE characteristic. Moreover, the enhancement of the fluorescence intensity was positively related to the activation state of T cells. Our study demonstrated the concept of cholesterol-derived AIE fluorescent probes for deciphering the spatiotemporal arrangements of TCR on the membrane during T cell activation, and consequently provided a novel and complementary strategy for detecting T cell activation in real-time.

1. Introduction

T cell based anti-tumor immunotherapy has achieved great clinical success, especially for the treatment of hematoma [1,2]. The key for a successful immunotherapy is the effective activation of T cells in tumor microenvironment [3,4]. Therefore, precise detection of T cell activation during immunotherapy is of great importance. On the one hand, the activated T cells generally change the expression of specific surface proteins, such as CD25, CD69, inducible T cell costimulatory and so on [5,6]. Methods focusing on detecting these cell-surface protein markers to reflect the activation of T cells have attracted a lot of interest, among which, flow cytometry, immunohistochemistry or immunofluorescence are the commonly used ones [7]. On the other hand, the activated T cells express cytokines, such as interferon-gamma (IFNγ), granzyme beta (GzmB), transforming growth factor beta (TGFβ), interleukin (IL)-2, IL-4, IL-17 et al., which are potential targets to prove the activation of T cells, but they tend to be transient, diffusible, and located in the extracellular matrix rather than on the T cells [8,9]. The methods focused on

* Corresponding author. State Key Laboratory of Natural Medicines, Jiangsu Key Laboratory of Drug Discovery for Metabolic Diseases, Jiangsu Key Laboratory of Drug Design and Optimization, Center of Advanced Pharmaceuticals and Biomaterials, China Pharmaceutical University, Nanjing, 210009, China.
** Corresponding author. State Key Laboratory of Natural Medicines, Jiangsu Key Laboratory of Drug Discovery for Metabolic Diseases, Jiangsu Key Laboratory of Drug Design and Optimization, Center of Advanced Pharmaceuticals and Biomaterials, China Pharmaceutical University, Nanjing, 210009, China.
E-mail addresses: haomeixi@cpu.edu.cn (M. Hao), zhangcan@cpu.edu.cn (C. Zhang).
[1] These authors contributed equally to this work.

https://doi.org/10.1016/j.ejmech.2022.115073
Received 5 October 2022; Received in revised form 18 December 2022; Accepted 28 December 2022
Available online 29 December 2022

detecting these cytokines include Enzyme-linked immunosorbent assay (ELISA), enzyme-linked immunosorbent spot assay (ELISpot), and so on [10,11]. However, most of the above-mentioned assays depend on the antibody-based technology, which require a tedious sample-preparation process, such as tissue dissociation, antibody incubation, multiple washing steps or culture medium collection [12,13]. Besides, the data fidelity may be limited due to the end-point assays of above methods [12], which cannot be used as real-time detected method. Although calcium-sensitive probes can detect T cell activation in real-time based on the calcium mobilization during activation, this approach is not feasible for long-term imaging due to the diffusion of calcium-sensitive probes [14]. Thus, simple, non-antibody-involved and real-time detection methods for characterizing the activation of T cells are still challenging.

It has been reported that T cell activation critically relies on the spatiotemporal arrangements of T cell receptor (TCR) on the membrane [15]. The spatial reorganization of the TCR into nanoclusters is involved in regulating T cell activity when T cells are activated [16,17]. The higher the degree of T cell activation, the more TCR nanoclusters [18]. Previous studies have also suggested that cholesterol is involved in the formation of TCR nanoclusters and aggregates with the formation of TCR nanoclusters [19]. Therefore, we hypothesized that the spatiotemporal arrangement of cholesterol on the membrane could be used to visualize TCR nanoclusters and evaluate the degree of T cell activation.

Recent years, many fluorescent probes have been designed to visualize TCR nanoclusters, however a high background luminescent noise signal are observed due to the fluorescence emission outside of the TCR nanoclusters [20,21]. Moreover, most of these fluorophores suffered from aggregation-caused quenching (ACQ) phenomenon, such as fluorescein, rhodamine, indocyanine green, and cyanine, which are either weakly emissive or non-emissive at high concentration or in the aggregation state [22,23]. It has reported that tetraphenylethene (TPE) structure possesses the aggregation-induced emission (AIE) character, of which fluorescence signal depends on its molecular concentration [24,25]. In other words, the TPE-derived agent is non-emissive in its molecularly dissolved form, but becomes emissive when in its aggregated form. To the best of our knowledge, there is no report of using fluorescent probes with AIE characteristic to visualize TCR nanoclusters and T cell activation so far.

Herein, we designed a series of novel cholesterol derived AIE probes (R-TPE-PEG-Chol). These probes consisted of a cholesterol anchor (Chol, the reddish-brown parts in Fig. 1A), the poly (ethylene glycol) chain (PEG, the yellow parts in Fig. 1A), and different polar hydrophilic R groups decorated TPE (R-TPE, the grey parts in Fig. 1A). The cholesterol anchor could mimic the membrane cholesterol, which could insert into the lipid bilayers of naïve T cell membrane *via* hydrophobic interactions and aggregate with the formation of TCR nanoclusters during T cell activation [26,27]. The PEG as the hydrophilic linker was introduced to improve the hydrophilicity of these probes, which led to the exposure of the R-TPE moiety to the extracellular space [11]. Additionally, the R groups with different polarity were introduced into the side chain of TPE to finely tune the polarity of these probes [28]. These probes could assess the activation state of T cells by visualizing TCR nanoclusters, which was achieved through monitoring the change of local probe concentration. In specific, R-TPE-PEG-Chol anchored to the naïve T cell membrane in its molecularly dissolved form, which was non-emissive since the probe displayed a decentralized state on the T cell membrane. Once T cells were activated, the TCR clustered, which led to the aggregation and fluorescence emission of R-TPE-PEG-Chol. The higher the activation degree of T cells, the higher the fluorescence intensity of these novel cholesterol derived AIE probes was found (Fig. 1B). Therefore, these novel cholesterol derived AIE probes could be used for visualizing the formation of TCR nanoclusters and detecting T cell activation in real-time.

2. Results and discussion

2.1. Chemistry

The synthetic route of the novel cholesterol derived AIE probes (R-TPE-PEG-Chol) were displayed in Scheme 1. Briefly, cholesterol hemisuccinate (cholesterol anchor, Chol) was first coupled with **Boc-PEG-**

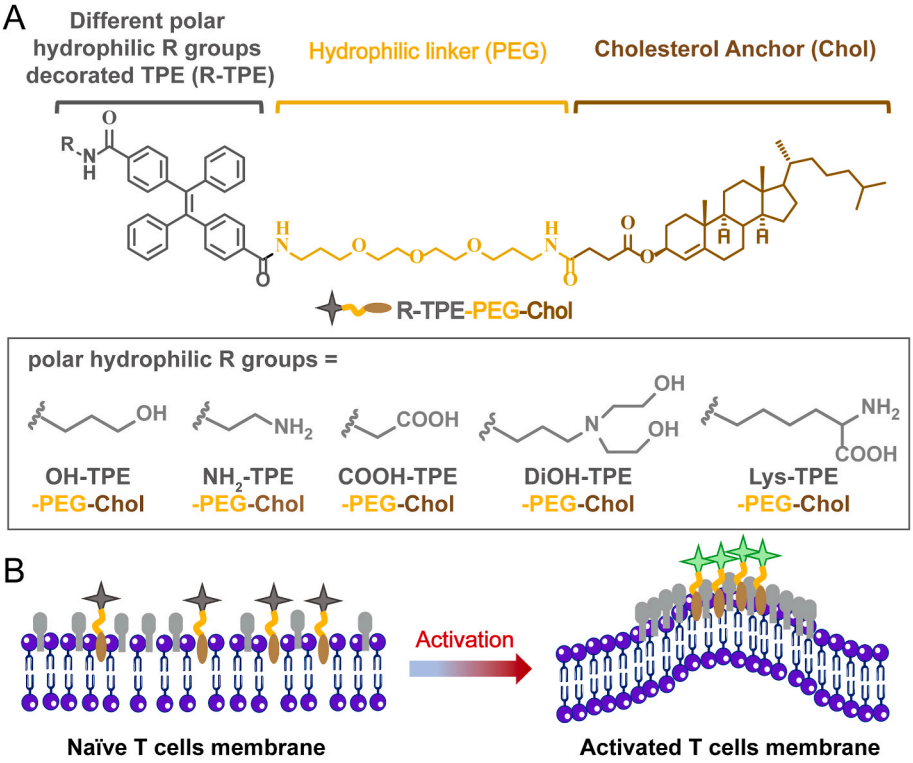

Fig. 1. Designed cholesterol derived AIE probes (R-TPE-PEG-Chol) for real-time monitoring the activation of T cells. (A) Design of R-TPE-PEG-Chol with cholesterol anchor, PEG hydrophilic linker and different polar hydrophilic R groups decorated TPE. (B) The working mechanism of R-TPE-PEG-Chol for monitoring of T cell activation by visualizing TCR nanoclusters. There is non-emissive since the probe is equally distributed in the naïve T cells membrane. Once T cells are activated, the formation of TCR nanoclusters will induce the AIE fluorescence since the probe aggregation occurs. The higher the activation of T cells, the more TCR nanoclusters, and the higher fluoresce intensity of R-TPE-PEG-Chol are found.

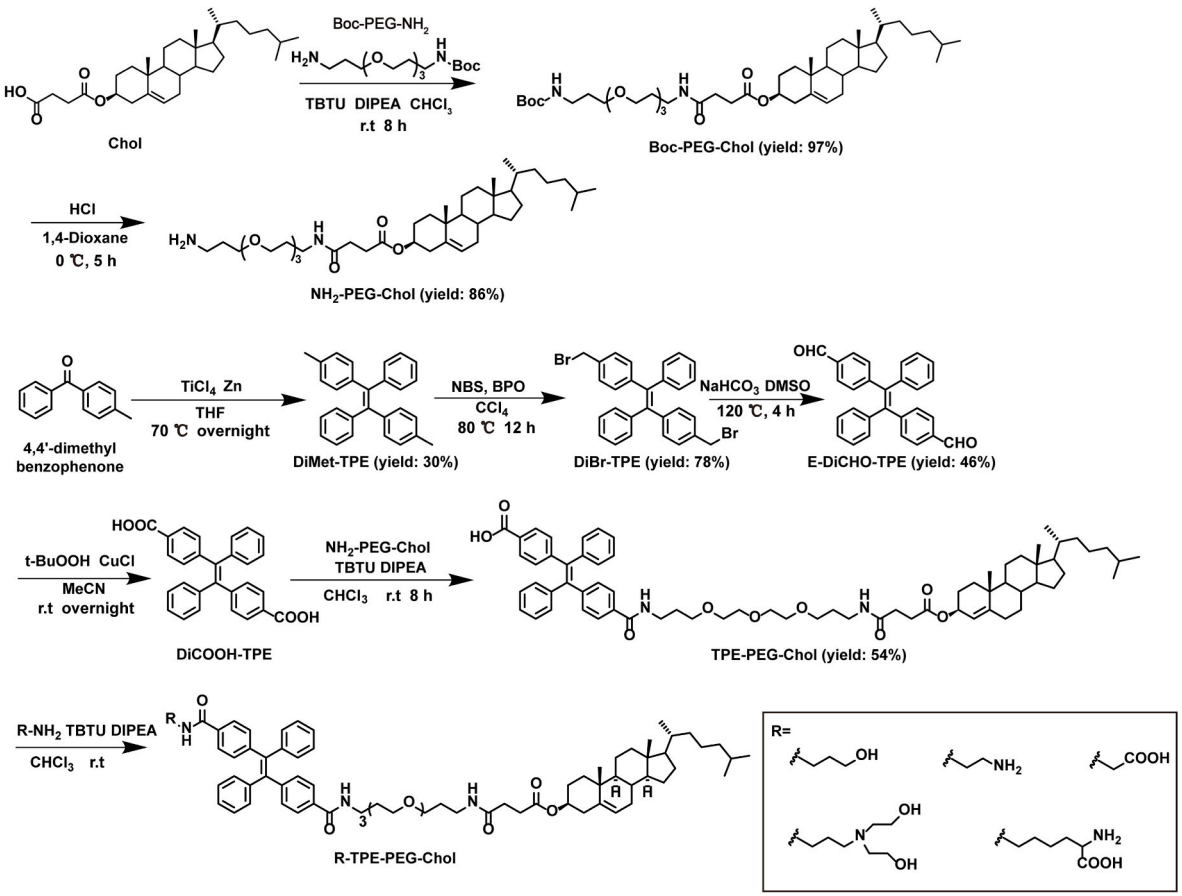

Scheme 1. The synthetic pathway of cholesterol derived AIE probes (R-TPE-PEG-Chol).

NH_2 in the presence of 2-(1*H*-Benzotriazole-1-yl)-1,1,3,3- tetramethyluronium tetrafluoroborate (TBTU) and *N*, *N*-Diisopropylethylamine (DIPEA) to afford compound **Boc-PEG-Chol**. Butyloxycarbonyl (Boc) was further discarded from **Boc-PEG-Chol** to afford intermediate **NH_2-PEG-Chol**. On the other hand, under the presence of $TiCl_4$ and Zn, 4-Methylbenzophenone accrued McMurry coupling reaction to afford **DiMet-TPE** containing TPE skeletons. Thorough bromination and hydrolysis, **DiMet-TPE** afforded mixture isomers **DiCHO-TPE**, which was further separated by column chromatography to afford the pure isomer of *E* and *Z* of **DiCHO-TPE**. Then, ***E*-DiCHO-TPE** was oxidized to afford intermediate **DiCOOH-TPE**. The intermediate **DiCOOH-TPE** reacted with intermediate **NH_2-PEG-Chol** to afford compound **TPE-PEG-Chol**. Finally, **TPE-PEG-Chol** reacted with **R–NH_2** to afford the targeted compounds **R-TPE-PEG-Chol** containing different R groups. All intermediates were characterized using ^{1}H NMR (Figs. S1–S6). Among them, *E* and *Z* isomer of **DiCHO-TPE** was further characterized using NOESY-NMR (Fig. S4). All R-TPE-PEG-Chol were characterized using ^{1}H NMR, ^{13}C NMR, high-resolution mass spectrometry (HRMS) and high-performance liquid chromatography (HPLC). The purities of the final probes were ≥95% according to HPLC and NMR analysis (Figs. S7–S11).

2.2. Detection of T cell activation by R-TPE-PEG-Chol

To verify the initial design concept, the photophysical properties of R-TPE-PEG-Chol were first investigated. The UV–vis absorption spectra of these probes were observed in dimethyl sulfoxide (DMSO) solution with two main absorption peaks at 290 nm and 330 nm (Fig. 2A and Fig. S12A). Moreover, the photophysical properties including excitation (Λex), emission (Λem), fluorescence quantum yields (Φ), Stokes' shift and the molar absorptivity coefficient of R-TPE-PEG-Chol in different solvent were presented in Fig. 2B and Fig. S13. These results implied that these designed probes possess excellent photophysical properties. Then, their AIE characteristics were studied by changing the water content of the water/DMSO mixtures. As presented in Fig. 2C–G and Fig. S12B, these probes had almost no emission in pure DMSO (a good solvent), and the addition of water (a poor solvent) to their DMSO solution induced the emergence of an emission peak, and the intensity progressively became higher with the increasing water content. Moreover, due to the twisted intramolecular charge transfer (TICT) effect, COOH-TPE-PEG-Chol (from 381 to 479 nm), DiOH-TPE-PEG-Chol (from 380 to 479 nm) and Lys-TPE-PEG-Chol (from 380 to 462 nm) showed a slight red-shift of emission when *fw* (%) increased from 0 to 40%, and NH_2-TPE-PEG-Chol (from 380 to 478 nm), OH-TPE-PEG-Chol (from 380 to 481 nm) showed red-shift of emission when *fw* (%) increased from 0 to 30% (Fig. 2C–G). These results suggested that these probes possessed typic AIE phenomenon, showing almost no emission in good solvent and strong fluorescence in poor solvent. Additionally, dynamic light scattering (DLS) data and Transmission Electron Microscope (TEM) imaging displayed that these probes aggregate into 100–1000 nm particles under aqueous environment, while no particle could be found in the MeOH (Fig. S14 and Fig. 2H). These results further indicated that these probes are dispersed in good solvent and aggregated in poor solvent. Taken together, it is fully proved that our designed probes do not emit in a dispersed state in good solvent, but emit strong fluorescence due to the molecular aggregation in poor solvent.

Since the cytotoxicity of R-TPE-PEG-Chol to T cells is an important parameter to determine whether it is suitable for T cell activation imaging, we evaluated the cytotoxicity of R-TPE-PEG-Chol before employing it for imaging T cell activation. The results showed that OH-TPE-PEG-Chol, COOH-TPE-PEG-Chol and DiOH-TPE-PEG-Chol had almost no cytotoxicity to T cells even at a concentration of 50 μM. However, NH_2-TPE-PEG-Chol and Lys-TPE-PEG-Chol displayed

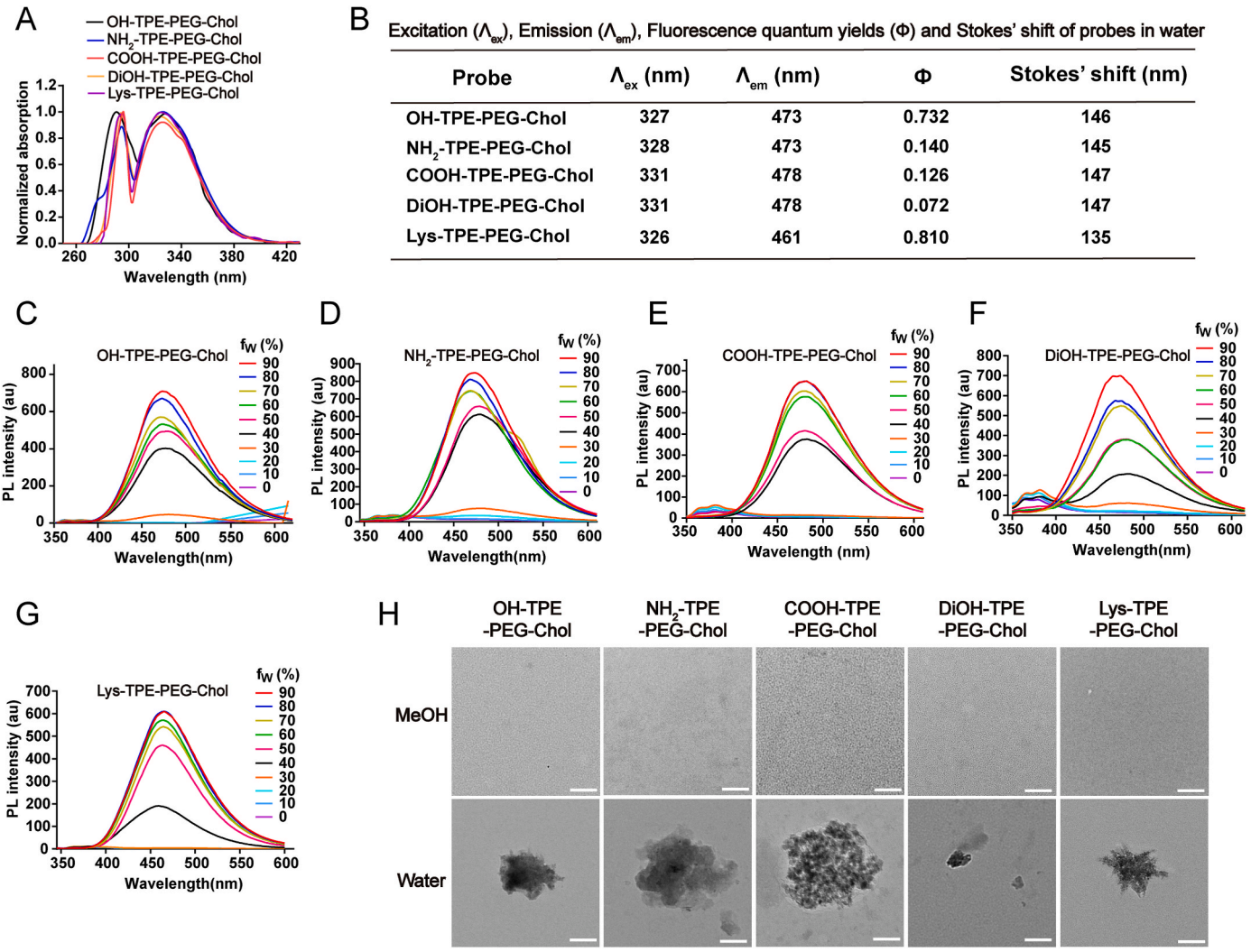

Fig. 2. Photophysical properties of R-TPE-PEG-Chol. (A) Normalized absorption spectra of R-TPE-PEG-Chol in pure DMSO. (B) Excitation, emission, fluorescence quantum yields and Stokes' shift of R-TPE-PEG-Chol in water. (C–G) Photoluminescence (PL) spectra of OH-TPE-PEG-Chol (C), NH_2-TPE-PEG-Chol (D), COOH-TPE-PEG-Chol (E), DiOH-TPE-PEG-Chol (F), Lys-TPE-PEG-Chol (G) in water/DMSO mixtures with different water fractions (*fw*). The concentration of R-TPE-PEG-Chol was 10 μM, and the excitation wavelength was 330 nm. (H) The TEM images of R-TEP-PEG-Chol in MeOH and water. The concentration of R-TEP-PEG-Chol was 10 μM. Scale bar: 100 nm.

significant cytotoxicity to T cells, and the cell viability was below 80% at the concentration of 4 μM, which may be attributed to the introduction of positively charged amino groups in both structures increasing the cytotoxicity to T cells (Fig. S15). Therefore, we choose 0–50 μM as the nontoxic concentration range of OH-TPE-PEG-Chol, COOH-TPE-PEG-Chol and DiOH-TPE-PEG-Chol, and 0–2.5 μM as the nontoxic concentration range of NH_2-TPE-PEG-Chol and Lys-TPE-PEG-Chol for further studies.

The anchoring of R-TPE-PEG-Chol to naïve T cells membrane is the premise for imaging T cell activation. Thus, we first screened the optimal anchoring concentration and time of these probes on naïve T cells by flow cytometry analysis under the nontoxic concentration range of R-TPE-PEG-Chol. The gating strategy of flow cytometry analysis was presented in Fig. S16. The results revealed that following the increase of anchoring concentration or time of R-TPE-PEG-Chol on T cells, the fluorescent intensities gradually increased after the T cell are activated. The optimal anchoring concentration and time were 10 μM and 20 min for OH-TPE-PEG-Chol, 20 μM and 20 min for DiOH-TPE-PEG-Chol, 20 μM and 30 min for COOH-TPE-PEG-Chol, 2.5 μM and 20 min for NH_2-TPE-PEG-Chol, and 2.5 μM and 10 min for Lys-TPE-PEG-Chol, respectively (Fig. S17 and Fig. S18). Moreover, we compared the mean fluorescence intensity (MFI) of T cells anchored with these probes at the optimal concentration and time after activated. The results displayed that T cells anchored with COOH-TPE-PEG-Chol had the strongest fluorescence intensity compared with other four probes (Fig. 3A and B). Based on the above results, we found that R-TPE-PEG-Chol bearing the higher polar chain and weaker hydrophobicity was easier to anchor to the surface of T cells and COOH-TPE-PEG-Chol was the optimal choice for evaluating the activation of T cells.

Next, we evaluated whether COOH-TPE-PEG-Chol affected the key cell functions of T cells. The results of trypan blue and CCK8 assays both displayed that viability of T cells anchored with COOH-TPE-PEG-Chol was higher than 85%, and there was no difference with the viability of the un-anchored T cells (Fig. 3C and D). The *in vitro* proliferative capacity of T cells anchored with COOH-TPE-PEG-Chol was unimpaired, and was comparable to that of un-anchored T cells (Fig. 3E). We next assessed the impact of COOH-TPE-PEG-Chol on the migration of T cells across the endothelial monolayer, which is the key function of T cells to infiltrate target tissues. The results displayed that the *trans*-endothelium migration capacity of T cells anchored with COOH-TPE-PEG-Chol did not decrease compared with un-anchored T cells (Fig. 3F). There was also no difference between the migration of anchored and un-anchored T

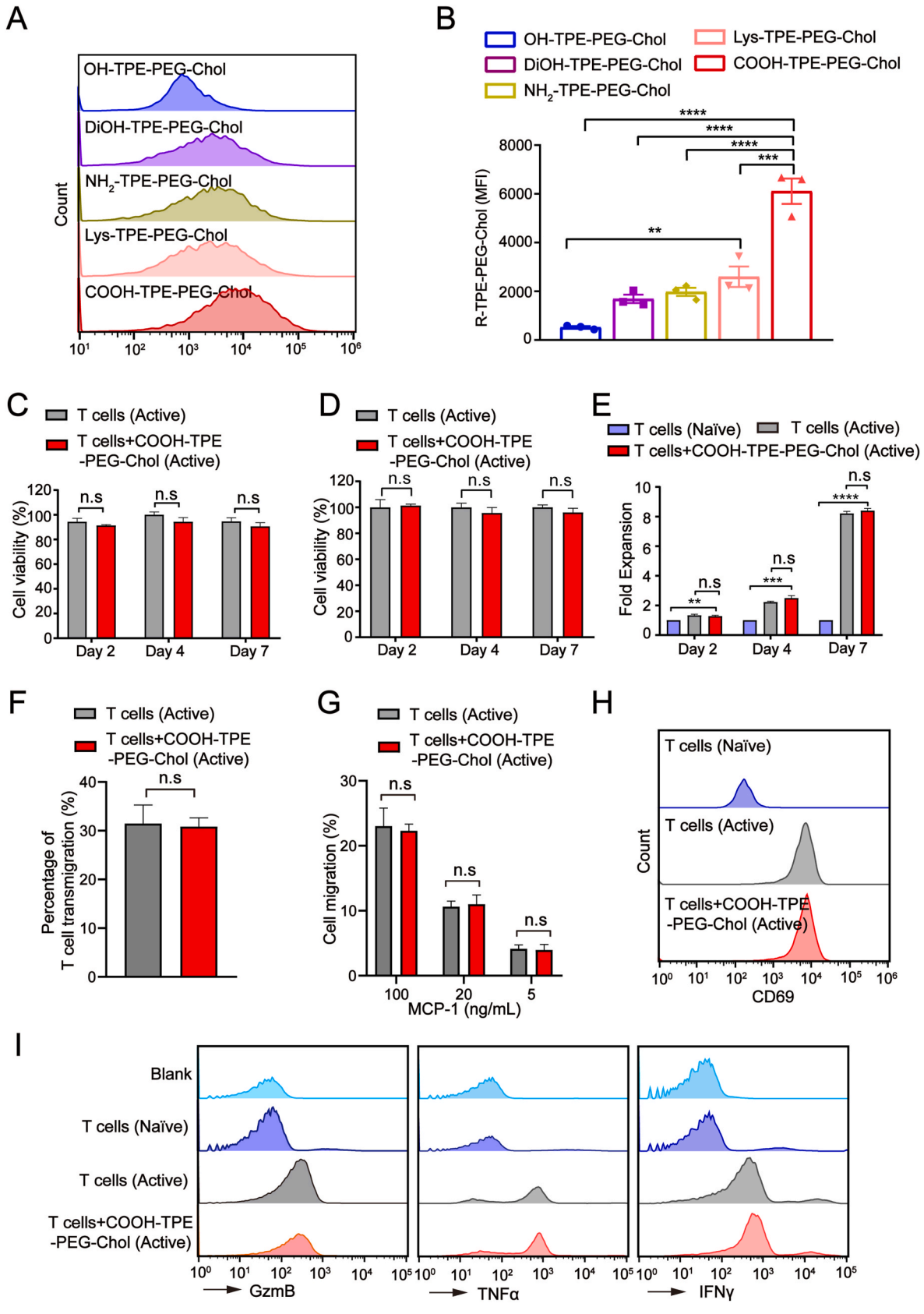

(caption on next page)

Fig. 3. Detection of activated T cells by R-TPE-PEG-Chol. (A) Flow cytometry analyze MFI of activated T cells under the optimal anchoring time and concentration. (B) Quantitative analysis in A). [OH-TPE-PEG-Chol *vs.* Lys-TPE-PEG-Chol (95% confidence interval (CI), −3560 to −593.1), OH-TPE-PEG-Chol *vs.* COOH-TPE-PEG-Chol (95% CI, −7075 to −4107), DiOH-TPE-PEG-Chol *vs.* COOH-TPE-PEG-Chol (95% CI, −5906 to −2939), NH_2-TPE-PEG-Chol *vs.* COOH-TPE-PEG-Chol (95% CI, 2652 to 5620), Lys-TPE-PEG-Chol *vs.* COOH-TPE-PEG-Chol (95% CI, 2031 to 4998)]. (C) Viability of T cells anchored with COOH-TPE-PEG-Chol for up to 7 days after stimulated with anti-CD3 and anti-CD28 antibody were evaluated by trypan blue assay. (D) Viability of T cells anchored with COOH-TPE-PEG-Chol for up to 7 days after stimulated with anti-CD3 and anti-CD28 antibody were measured by CCK8 assay. (E) *In vitro* expansion of T cells anchored with COOH-TPE-PEG-Chol after stimulated with anti-CD3 and anti-CD28 antibody, the naïve and activated T cells were used as controls. [Day 2 T cells (Naïve) *vs.* Day 2 T cells + COOH-TPE-PEG-Chol (Active) (95% CI, −0.5028 to −0.05717), Day 4 T cells (Naïve) *vs.* Day 4 T cells + COOH-TPE-PEG-Chol (Active) (95% CI, −1.943 to −10.43), Day 7 T cells (Naïve) *vs.* Day 7 T cells + COOH-TPE-PEG-Chol (Active) (95% CI, −7.928 to −6.878)]. (F) The *trans*-endothelium migration capacity of T cells anchored with COOH-TPE-PEG-Chol after stimulated with anti-CD3 and anti-CD28 antibody. (G) The chemotaxis migration behaviors of T cells anchored with COOH-TPE-PEG-Chol after stimulated with anti-CD3 and anti-CD28 antibody. (H) Flow cytometry analysis of cell surface CD69 expression, naïve T cells were used as control. (I) Expression of inflammatory cytokines measured by flow cytometry. The concentration of OH-TPE-PEG-Chol, DiOH-TPE-PEG-Chol, COOH-TPE-PEG-Chol, NH_2-TPE-PEG-Chol and Lys-TPE-PEG-Chol used for incubation with naïve $CD8^+$T cells in A) were 10 μM, 20 μM, 20 μM, 2.5 μM and 2.5 μM, respectively. The concentration of COOH-TPE-PEG-Chol used for incubation with naïve $CD8^+$T cells in C–I) was 20 μM. Error bars denote SEM. $^*P < 0.05$, $^{**}P < 0.01$, $^{***}P < 0.001$, $^{****}P < 0.0001$, n.s denotes no significant difference.

cells in response to chemoattractant (Fig. 3G). The T cell activation signaling molecules were analyzed by Western bolt, and the activation marker and cytokine secretion of T cells were also analyzed by flow cytometry and the gating strategy was displayed in Fig. S19 and Fig. S20. The data displayed that the anchored COOH-TPE-PEG-Chol did not affect the activation of T cells by testing the expression of CD69 marker (Fig. 3H). The immunoblot analysis result showed that anchoring COOH-TPE-PEG-Chol did not affect the expression of activation signaling molecules, including phosphorylation of CD3ζ (pCD3ζ) and phosphorylation of the zeta chain of T cell receptor-associated protein kinase 70 (pZAP70), which were not significantly different from un-anchored T cells (Fig. S21A). Last but not least, there was no obvious difference on the secretion of cytokine such as IFNγ, GzmB and transforming growth factor α (TNFα) of anchored T cells, when compared to that of un-anchored T cells, indicating that the anchored COOH-TPE-PEG-Chol had no effect on expression of cytokine by T cells (Fig. 3I and Fig. S21B). Together, COOH-TPE-PEG-Chol had no influence on the key cellular functions of T cells, and it was safe to assess the activation of T cells.

2.3. Real-time monitoring the activation of T cells by COOH-TPE-PEG-Chol

Previous studies have reported that the distribution of cholesterol in cell membrane was related to the activation of T cells [11,19,29]. Thus, we first isolated the naïve $CD8^+$T cells from the spleen of mice and evaluated the cholesterol distribution in naïve and activated T cell membrane, and stained the cell membrane cholesterol by Filipin III [11]. As shown in Fig. 4A, Figs. S22A and B, cholesterol displayed a decentralized state on naïve T cells and aggregate state on activated T cells. We further imaged TCR clustering and probe aggregation on naïve and activated $CD8^+$T cells. The result displayed that the red fluorescence of TCR was aggregated after T cell activated, implying that the nanocluster of TCR was formed on activated T cells. Additionally, the aggregated red fluorescence of TCR nanocluster and the green fluorescence of COOH-TPE-PEG-Chol were overlapped very well with a correlation coefficient of 0.82 on activated T cells membrane, while there was no green fluorescence on naïve T cells membrane (Fig. 4B–E, Figs. S22C and D). As the activation time of T cells increased, the fluorescence of COOH-TPE-PEG-Chol gradually increased (Fig. 4F and G). The signal-to-noise ratio of probe was 590 ± 30, and the signal-to-background ratio of probe was 660 ± 30, indicating our designed probe has a high signal-to-noise ratio. Moreover, the lifetime of COOH-TPE-PEG-Chol on the cell surface is longer than 96 h (Fig. S23), indicating the cholesterol probe could image the activation of T cells for a long time. Together, these results confirmed that COOH-TPE-PEG-Chol could specifically aggregate and fluoresce in the TCR nanoclusters of activated T cells and assess the activation of T cells in real time.

We next evaluated the efficacy of designed probe for real-time monitoring human T cell activation. The naïve human $CD8^+$T cells were isolated from the peripheral blood of healthy donors, and anchored with probe and then activated with different concentrations of anti-CD3 antibody or anti-CD3 antibody plus anti-CD28 antibody, where the higher the concentration of anti-CD3 antibody and anti-CD28 antibody, the higher the degree of T cell activation [30]. The result of flow cytometry assay showed that as the degree of T cell activation increased, the fluorescence intensity of COOH-TPE-PEG-Chol increased (Fig. 5A and B). These results were further confirmed by confocal imaging in which activated human T cells showed the green fluorescence of COOH-TPE-PEG-Chol, while naïve T cells had no fluorescence. Besides, as the antibody concentration increased, the degree of T cell activation increased, and the green fluorescence of COOH-TPE-PEG-Chol on human T cell membrane became stronger (Fig. 5C, D and Fig. S24). Similar to murine T cells, these results indicated that probe had the ability to monitor human T cell activation.

As we all know, activated T cells was gradually exhaustion in tumor immunosuppressive microenvironment, we further obtained ovarian cancer tissue from patient, and used this tissue to simulate the immunosuppressive environment for further investigating the real-time imaging ability of COOH-TPE-PEG-Chol [31,32]. The naïve human $CD8^+$T cells anchored with COOH-TPE-PEG-Chol were activated with anti-CD3 and anti-CD28 antibody. Then the activated $CD8^+$T cells were injected into the cancer tissue and incubated for different times. As shown in Fig. 5E and Fig. S25, with the extension of incubation time, the $CD8^+$T cells gradually exhausted in the cancer tissue, and the expression of pZAP70, iconic marker for the activation T cells [33], gradually decreased and was almost invisible in $CD8^+$T cells after 8 h. Meanwhile, the green fluorescence of COOH-TPE-PEG-Chol, co-localized with pZAP70 in $CD8^+$T cells, also decreased over time. These data implied that the most of activated $CD8^+$T cells in ovarian cancer tissue inactivate as time went on, and COOH-TPE-PEG-Chol could real-time image T cells with different activation levels. In addition, the fluorescence of COOH-TPE-PEG-Chol in $CD8^+$T cells could be observed for more than 24 h compared to pZAP70 which was almost unobservable after 8 h. This meant that COOH-TPE-PEG-Chol could more accurately real-time image $CD8^+$T cells with heterogeneous activation levels compared to commercially available antibodies. Together, our designed probe has potential market value and clinical application prospects for real-time monitoring the *in vivo* fate of T cells.

3. Conclusion

T cells are an important component of the adaptive immune response and have direct cytotoxic and immune-modulating functions [34]. Currently, the T cells immunotherapy has achieved remarkable success in hematologic tumors [1,2]. The key for a successful immunotherapy in solid tumor is the effective activation of T cells in tumor microenvironment [35]. Thus, it is of great significant to accurately detect the activation of T cells in real time. However, these real time detection methods are lacking. It is well known that the activation of T cells

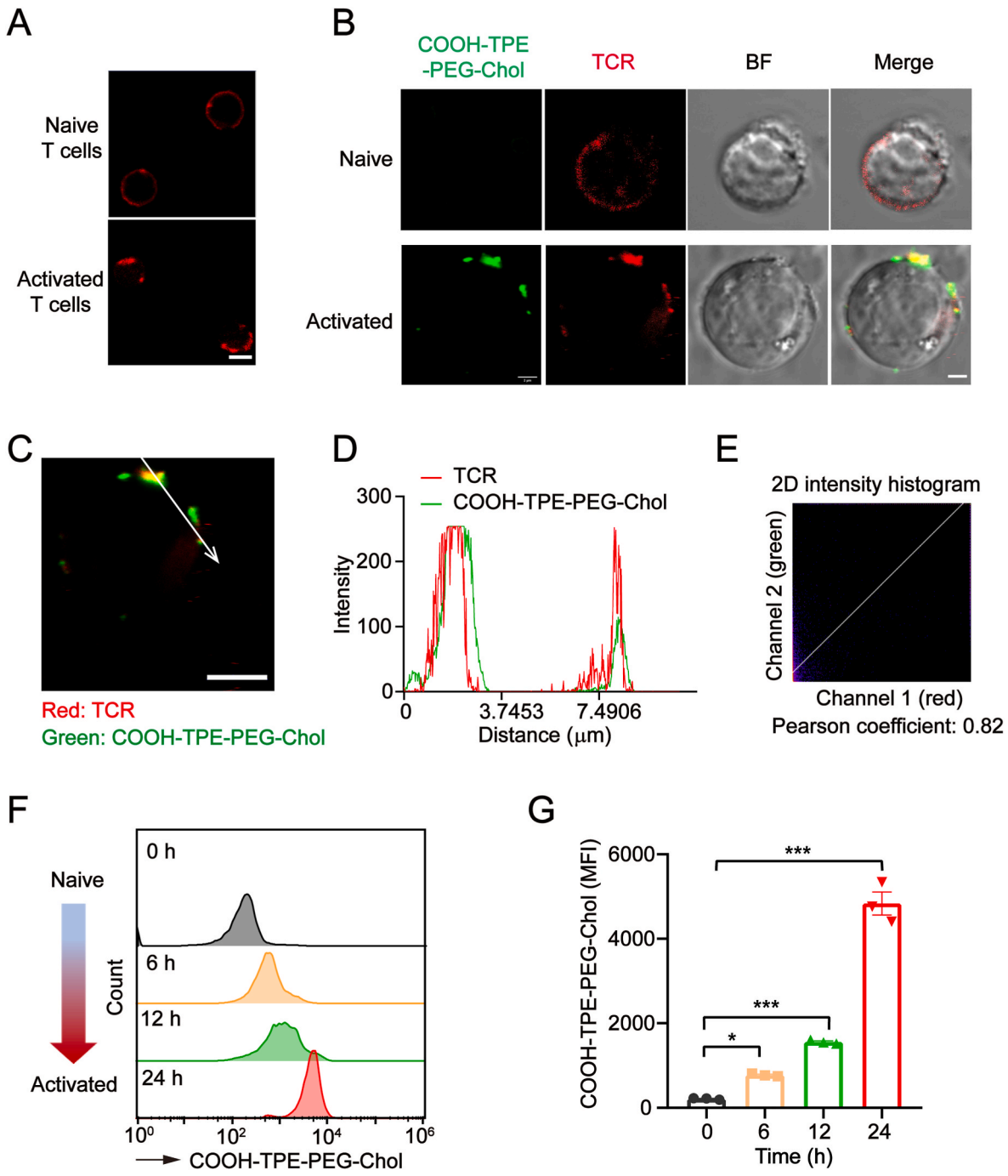

Fig. 4. Real-time monitoring the activation of T cells by COOH-TPE-PEG-Chol. (A) Cholesterol distribution on naïve and activated $CD8^+$T cells by Filipin III staining. Scale bar: 10 μm. (B) Monitoring the activation of T cell with COOH-TPE-PEG-Chol and Alexa Fluor 647 anti-TCR antibody by CLSM imaging. Scale bar: 2 μm. (C) Colocalization of COOH-TPE-PEG-Chol and TCR nanoclusters on activated T cells observed by CLSM imaging. (D) Profile analysis for evaluation of co-localization of COOH-TPE-PEG-Chol and TCR in C). (E) 2D intensity histogram output of coloc2 analysis performed with Fiji/ImageJ. The text indicates the classical Pearson coefficient of the pixel-intensity correlation. (F) Real-time monitoring the activation of T cell with COOH-TPE-PEG-Chol by flow cytometry analyze. (G) Quantitative analysis in F). [0 h *vs.* 6 h (95% CI, −1123 to −2.668), 0 h *vs.* 12 h (95% CI, −1905 to −784.7), 0 h *vs.* 24 h (95% CI, −5183 to −4063)]. The concentration of COOH-TPE-PEG-Chol used for incubation with naïve $CD8^+$T cells in B-G) was 20 μM. Error bars denote SEM. $^*P < 0.05$, $^{***}P < 0.001$.

accompanied with TCR aggregation and the formation of TCR nanocluster, which also lead to the aggregation of cholesterol on the T cells membrane [16,17,19].

Based on this, we designed and synthesized five cholesterol derived AIE probes (R-TPE-PEG-Chol), which bear cholesterol anchor as a membrane cholesterol mimic, PEG as the hydrophilic linker and TPE with different polar hydrophilic groups on the side chain. A comprehensive series of experiments were performed to validate their AIE character and assess their effect of imaging the activation state of T cells. Among the five probes, COOH-TPE-PEG-Chol possessed the best imaging effect on activated T cells and did not influence the key physiological functions of T cells. With the extension of activation time, COOH-TPE-PEG-Chol could monitor the activation process of T cells in real time. Moreover, COOH-TPE-PEG-Chol enabled real-time assessment of T cells with heterogeneous activation states while minimizing background interference from free dyes and autofluorescence of biological

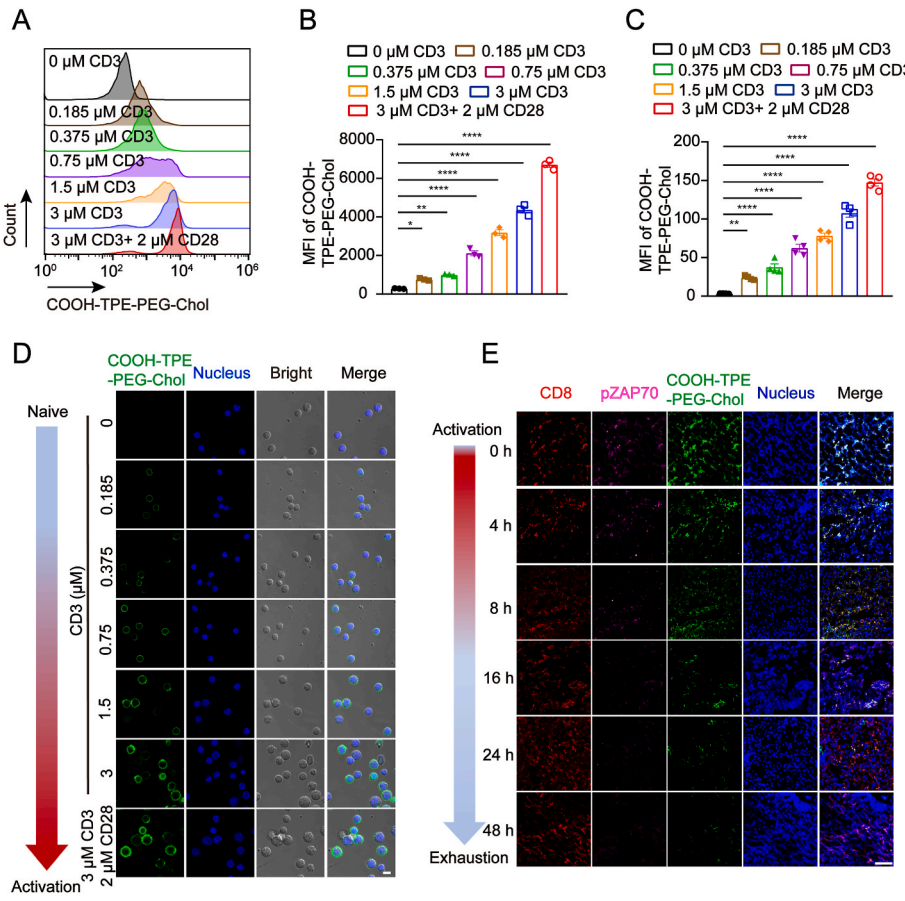

Fig. 5. Real-time imaging the activation of human T cells by COOH-TPE-PEG-Chol. (A) Flow cytometry analysis of fluorescence intensity of COOH-TPE-PEG-Chol anchored human $CD8^+$T cells after stimulated with different concentration of CD3 and CD28 antibody. (B) Quantitative analysis in A). [0 μM CD3 *vs.* 0.185 μM CD3 (95% CI, −940.0 to −19.28), 0 μM CD3 *vs.* 0.375 μM CD3 (95% CI, −1172 to −251.6), 0 μM CD3 *vs.* 0.75 μM CD3 (95% CI, −2295 to −1374), 0 μM CD3 *vs.* 1.5 μM CD3 (95% CI, −3357 to −2436), 0 μM CD3 *vs.* 3 μM CD3 (95% CI, −4537 to −3616), 0 μM CD3 *vs.* 3 μM CD3+2 μM CD28 (95% CI, −6883 to −5962)]. (C) Quantitative analyze the fluorescence intensity of COOH-TPE-PEG-Chol in activated human $CD8^+$T cells for confocal imaging. [0 μM CD3 *vs.* 0.185 μM CD3 (95% CI, −35.93 to −4.767), 0 μM CD3 *vs.* 0.375 μM CD3 (95% CI, −49.68 to −18.52), 0 μM CD3 *vs.* 0.75 μM CD3 (95% CI, −74.43 to −43.27), 0 μM CD3 *vs.* 1.5 μM CD3 (95% CI, −90.18 to −59.02), 0 μM CD3 *vs.* 3 μM CD3 (95% CI, −119.9 to −88.77), 0 μM CD3 *vs.* 3 μM CD3+2 μM CD28 (95% CI, −159.7 to −128.5)]. (D) The confocal imaging of COOH-TPE-PEG-Chol anchored naïve human $CD8^+$T cells were stimulated with different concentration of CD3 and CD28 antibody. Scale bar: 10 μm. (E) Real-time monitoring human $CD8^+$T cells with heterogeneous activation levels in suppressive microenvironment by COOH-TPE-PEG-Chol. Scale bar: 100 μm. The concentration of COOH-TPE-PEG-Chol used for incubation with naïve $CD8^+$T cells was 20 μM. Error bars denote SEM. $^*P < 0.05$, $^{**}P < 0.01$, $^{****}P < 0.0001$.

substrates.

In conclusion, we developed a novel cholesterol derived AIE probe for real-time monitoring the activation of adoptive T cells. This probe is simple, safe and has high spatial and temporal resolution that is amenable with live cell assessment, longitudinal studies. However, due to the short penetration depth of light, the application of detecting activation of adoptive T cells *in vivo* is limited. In the future, probes with large light penetration depth for detecting adoptive T cells *in vivo* can be developed. For example, structure with high excitation wavelength and AIE character can be used instead of TPE structure. Our study demonstrated the concept of cholesterol-derived AIE fluorescent probes for visualizing the spatiotemporal arrangements of TCR on the membrane during T cell activation, and consequently opened a novel and complementary avenue for detecting T cell activation. We expect this concept will be used for real-time detecting the adoptive T cells *in vivo*, and serve for the efficacy evaluation of T cell immunotherapies.

4. Materials and methods

4.1. General procedure for the synthesis of R-TPR-PEG-Chol

4.1.1. Synthesis of compound Boc-PEG-Chol

Cholesteryl hemisuccinate (Chol, 2 g, 4 mmol) and 2-(1*H*-Benzotriazole-1-yl)-1,1,3,3-tetramethyluronium tetrafluoroborate (TBTU, 1.29 g, 4 mmol) were dissolved in 100 mL of $CHCl_3$ with *N*, *N*-Diisopropylethylamine (DIEA, 860 μL, 5.2 mmol). Then 1-(BOC-amino)-13-amino-4,7,10-trioxa-tridecane (Boc-PEG-NH_2, 1.22 g, 4 mmol) was added to the solution. The mixture was stirred at room temperance for 8 h, then it was evaporated in vacuo. The crude product was purified by column chromatography ($CHCl_2$: MeOH = 20: 1) to give compound Boc-PEG-Chol as a white solid (2.95 g, 97% yield). ^{1}H NMR (300 MHz, $CDCl_3$) δ: 4.99 (1H, s), 4.61 (1H, s), 3.64–3.46 (10 H, m), 3.35 (2 H, dd, J = 12.1, 6.1 Hz), 3.21 (2 H, d, J = 5.9 Hz), 2.79 (2 H, s), 2.62 (2 H, t, J = 6.6 Hz), 2.43–2.31 (2 H, t, J = 6.8 Hz), 2.30 (2 H, d, J = 8.0 Hz), 2.10–1.74 (8 H, m), 1.68–1.12 (20 H, m), 0.92 (23 H, ddd, J = 21.2, 17.6, 10.6 Hz), 0.67 (3 H, s).

4.1.2. Synthesis of intermediate NH_2-PEG-Chol

2 M Hydrogen chloride-1,4-Dioxane solution was added into bottle containing compound Boc-PEG-Chol (2.9 g, 3.8 mmol) drop by drop at 0 °C and the mixture was stirred for 5 h. The solution was evaporated in vacuo. Water (80 mL) was added to the residue followed by adjustment of the pH to neutral. The aqueous solution was extracted with 200 mL dichloromethane and the organic layers were dried over Na_2SO_4, filtered, and concentrated to yield the final crude product as a brown solid (2.19 g, 86% yield) which was directly used in the next reaction without further purification.

4.1.3. Synthesis of compound DiMet-TPE

Into a 500 mL two-necked round-bottom flask with a reflux condenser was placed zinc dust (Zn, 10 g, 150 mmol). The flask was evacuated under vacuum and flushed with dry nitrogen three times. 100 mL of dry THF was then added. The mixture was cooled to −30 °C and $TiCl_4$ (8 mL, 75 mmol) was slowly added. The mixture was slowly warmed to room temperature, stirred for 0.5 h, then refluxed for 2 h. After stirring for 10 min, a solution of 4,4′-dimethylbenzophenone (10 g, 48 mmol) in 200 mL dry THF was added. Then, the mixture was refluxed overnight. The reaction was quenched with 10% K_2CO_3 aqueous solution until the solid turned to grey. The mixture was extracted with dichloromethane three times and the organic layers were combined and washed with brine twice. Solvent was evaporated under reduced pressure and the crude product was purified on a silica-gel column ($CHCl_2$:

MeOH = 20: 1). A yellow solid was obtained in 30% yield. ^{1}H NMR (300 MHz, $CDCl_3$) δ: 7.12–7.04 (10 H, m), 6.94, 6.91 (8 H, d, J = 7.0 Hz), 2.28, 2.27 (6 H, d, J = 5.4 Hz).

4.1.4. Synthesis of compound DiBr-TPE

In a 100 mL round bottom flask, a solution of compound DiMet-TPE (5.76 g, 16 mmol), *N*-bromosuccinimide (NBS, 2.84 g, 16 mmol), 400 mg of benzoyl peroxide (BPO) in 250 mL of CCl_4 was refluxed for 12 h. After the reaction was completed, the mixture was extracted with dichloromethane and water. The combined organic layers were dried over magnesium sulfate, and removed under reduced pressure. The crude product was purified by silica-gel chromatography to give compound DiBr-TPE as white solid (6.50 g, 78% yield). ^{1}H NMR (500 MHz, $CDCl_3$) δ: 7.14–7.08 (8 H, m), 7.04–6.97 (6 H, m), 6.91, 6.90 (4 H, d, J = 5.0 Hz), 4.43, 4.41 (2 H, d, J = 10.0 Hz), 4.15–4.11 (2 H, q, J = 7.1 Hz).

4.1.5. Synthesis of compound E-DiCHO-TPE

Compound DiBr-TPE (6.21 g, 11.98 mmol) and sodium carbonate ($NaHCO_3$, 3.12 g, 37.10 mmol) were dissolved in 25 mL dimethyl sulfoxide (DMSO). The solution was stirred at 120 °C for 4 h and then the solvent was evaporated in vacuo. The brown solid was extracted with dichloromethane and then the organic layers were dried over Na_2SO_4, filtered, and concentrated to obtain the mixture isomers which was purified by silica column chromatography ($CHCl_2$: MeOH = 40:1) to yield compound *E*-DiCHO-TPE as yellow solid (2.81 g, 46% yield) and *Z*-DiCHO-TPE as yellow solid. *E*-DiCHO-TPE: ^{1}H NMR (500 MHz, $CDCl_3$) δ: 9.91 (2 H, s), 7.63 (4 H, d, J = 8.1 Hz), 7.23–7.11 (10 H, m), 7.00 (4 H, d, J = 7.1 Hz). Z-DiCHO-TPE: ^{1}H NMR (500 MHz, $CDCl_3$) δ: 9.92 (2 H, s), 7.63 (4 H, d, J = 8.1 Hz), 7.22–7.11 (10 H, m), 7.03–6.96 (4 H, m). Moreover, the NOESY-NMR results displayed that the cross-peaks at the intersection of red dotted lines indicate clear correlations between H7/H11/H12/H16 and H18/H19/H20/H23/H24/H25 in the *E*-DiCHO-TPE, indicating that ring B and ring D are close in space, that is, on the same side of the central double bond. At the same time, we cannot find clear correlations between H7/H11/H12/H16 and H18/H19/H20/H23/H24/H25 in the *Z*-DiCHO-TPE because ring B is far from ring D.

4.1.6. Synthesis of DiCOOH-TPE

Compound *E*-DiCHO-TPE (1.91 g, 4.88 mmol) and 6 M *tert*-butyl hydroperoxide (t-BuOOH, 270 μL, 14.6 mmol) were dissolved in 4 mL acetonitrile. The solution was reacted at room temperature overnight. The reaction was quenched with saturated sodium hydrogen sulfite solution, followed by extraction with ethyl acetate and then the organic layers were dried over Na_2SO_4, filtered, and concentrated. The obtained crude product was purified by silica column chromatography to yield DiCOOH-TPE as yellow solid. ^{1}H NMR (500 MHz, $CDCl_3$) δ: 8.10, 8.08 (4 H, d, J = 5.4 Hz), 7.84, 7.82 (2 H, d, J = 8.4 Hz), 7.36, 7.35 (2 H, d, J = 2.5 Hz), 7.29, 7.28 (1 H, d, J = 2.0 Hz), 7.14–6.99 (9 H, m).

4.1.7. Synthesis of intermediate TPE-PEG-Chol

DiCOOH-TPE (860 mg, 2.0 mmol) and TBTU (857 mg, 2.7 mmol) were dissolved in 30 mL of $CHCl_3$, and DIEA (440 μL, 2.7 mmol) was added. Then the intermediate NH_2-PEG-Chol (1.52 g, 2.3 mmol) was added to the solution. The mixture was stirred at room temperature for 8 h, then it was evaporated in vacuo. The crude product was purified by column chromatography ($CHCl_2$: MeOH = 50: 1) to afford intermediate TPE-PEG-Chol (1.16 g, 54% yield) as a white solid. ^{1}H NMR (500 MHz, $CDCl_3$) δ: 7.64–7.52 (3 H, m), 7.50, 7.48 (2 H, dd, J = 15.6, 7.7 Hz), 7.24–7.20 (6 H, m), 7.15, 7.14 (2 H, d, J = 8.3 Hz), 7.08, 7.07 (5 H, dd, J = 6.2, 2.8 Hz), 5.34 (1 H, d, J = 3.9 Hz), 4.59 (1 H, m), 3.69 (6 H, s), 3.57–3.59 (4 H, t, J = 5.6 Hz), 3.54–3.52 (4 H, t, J = 6.1 Hz), 3.38–3.33 (2 H, q, J = 6.2 Hz), 2.66–2.64 (2H, t, J = 7.0 Hz), 2.49–2.48 (2 H, t, J = 6.9 Hz), 2.36, 2.34 (2 H, d, J = 7.8 Hz), 2.06–1.93 (2 H, m), 1.92–1.78 (5 H, m), 1.77–1.65 (2 H, m), 1.62–1.48 (12 H, m), 1.21–1.12 (6 H, m), 1.06–0.92 (5 H, m), 0.90 (10 H, ddd, J = 10.1, 8.5, 4.5 Hz), 0.67 (3 H, s).

4.1.8. Synthesis of target compound OH-TPE-PEG-Chol

TPE-PEG-Chol (76.3 mg, 0.07 mmol) and TBTU (25.5 mg, 0.08 mmol) were dissolved in 30 mL of $CHCl_3$, and DIEA (14 μL, 0.09 mmol) was added. Then the monoethanolamine (6 μL, 0.08 mmol) was added to the solution. The mixture was stirred at room temperature for 8 h, then it was evaporated in vacuo. The crude product was purified by column chromatography ($CHCl_2$: MeOH = 20: 1) to afford target compound OH-TPE-PEG-Chol (27.3 mg, 34% yield) as a white solid. HRMS, ESI$^+$, *m/z*: calcd for $C_{72}H_{97}N_3O_9$ $(M + H)^+$ 1148.72976, found 1148.73033. ^{1}H NMR (500 MHz, $CDCl_3$) δ: 7.58–7.52 (4 H, t, J = 8.6 Hz), 7.12–7.06 (10 H, m), 7.00, 6.99 (4 H, d, J = 3.6 Hz), 5.37, 5.35 (1 H, d, J = 4.2 Hz), 4.68–4.48 (1 H, m), 3.72–3.69 (10 H, t, J = 5.4 Hz), 3.65, 3.63 (4 H, d, J = 7.4 Hz), 3.58–3.47 (4 H, dt, J = 11.7, 7.2 Hz), 3.33, 3.31 (2 H, dd, J = 12.1, 6.1 Hz), 2.64–2.59 (2 H, t, J = 6.7 Hz), 2.46–2.41 (2 H, t, J = 6.8 Hz), 2.33–2.30 (2 H, t, J = 8.6 Hz), 1.87–1.84 (3 H, t, J = 14.3 Hz), 1.78 (9 H, ddd, J = 22.0, 11.6, 5.7 Hz), 1.64–1.50 (7 H, m), 1.09 (6 H, dd, J = 16.8, 7.5 Hz), 0.94, 0.92 (5 H, d, J = 8.7 Hz), 0.89, 0.87 (12 H, dd, J = 14.5, 6.5 Hz), 0.69 (3 H, d, J = 8.5 Hz). ^{13}C NMR (75 MHz, $CDCl_3$) δ: 172.36, 171.38, 168.02, 166.93, 146.89, 146.83, 146.47, 142.68, 141.16, 141.05, 141.01, 140.89, 139.59, 132.82, 132.69, 132.29, 132.24, 132.11, 131.36, 131.22, 131.15, 128.05, 127.94, 127.10, 126.98, 126.44, 126.37, 122.58, 74.26, 70.43, 70.22, 69.98, 69.77, 59.82, 56.66, 50.02, 42.28, 39.70, 39.46, 38.68, 38.04, 37.77, 37.11, 36.93, 36.55, 36.14, 35.71, 33.64, 32.12, 31.83, 31.07, 29.92, 29.60, 29.38, 29.26, 29.19, 28.96, 28.14, 27.93, 27.70, 24.76, 24.22, 23.78, 22.71, 22.59, 22.47, 20.98, 19.23, 18.66, 11.79.

4.1.9. Synthesis of target compound COOH-TPE-PEG-Chol

TPE-PEG-Chol (89.1 mg, 0.08 mmol) and TBTU (39.3 mg, 0.09 mmol) were dissolved in 30 mL of $CHCl_3$, and DIEA (51 μL, 0.33 mmol) was added. Then the glycine methyl ester hydrochloride (7.2 mg, 0.08 mmol) was added to the solution. The mixture was stirred at room temperature for 8 h, then it was evaporated in vacuo. The crude product was purified by column chromatography ($CHCl_2$: MeOH = 20: 1) to afford white solid. Then the white solid was dissolved in 2 mL trifluoroacetic acid (TFA) and was stirred at room temperature for 3 h. The reaction was quenched with saturated sodium hydrogen sulfite solution, followed by extraction with ethyl acetate and then the organic layers were dried over Na_2SO_4, filtered, and concentrated. The obtained crude product was purified by silica column chromatography to yield the target compound COOH-TPE-PEG-Chol (29.4 mg, 32% yield) as white solid. HRMS, ESI$^+$, *m/z*: calcd for $C_{71}H_{93}N_3O_{10}$ $(M + H)^+$ 1148.69337, found 1148.69205. ^{1}H NMR (500 MHz, $CDCl_3$) δ: 7.56–7.51 (4 H, m), 7.09–6.89 (14 H, m), 5.35 (1 H, d, J = 4.5 Hz), 4.64–4.50 (1 H, m), 3.60 (3 H, s), 3.54–3.29 (14 H, m), 3.18 (1 H, s), 2.59 (2 H, t, J = 7.2 Hz), 2.42 (2 H, dd, J = 19.9, 12.8 Hz), 2.29 (2 H, dd, J = 15.7, 7.9 Hz), 2.02–1.90 (3 H, m), 1.85–1.76 (3 H, m), 1.70 (1 H, dd, J = 12.0, 5.9 Hz), 1.53–1.43 (8 H, m), 1.13–1.08 (5 H, m), 0.90 (22 H, dddd, J = 18.5, 17.2, 14.0, 10.1 Hz), 0.67 (3 H, d, J = 4.6 Hz). ^{13}C NMR (126 MHz, $CDCl_3$) δ: 172.52, 172.37, 171.89, 149.19, 149.16, 146.26, 145.46, 142.81, 142.73, 141.00, 139.65, 138.98, 131.23, 131.16, 129.71, 128.03, 127.97, 127.82, 126.93, 126.89, 126.51, 124.35, 123.44, 122.61, 119.02, 118.87, 74.23, 70.45, 70.26, 70.15, 70.04, 69.80, 64.00, 56.70, 56.19, 49.59, 42.64, 41.64, 39.74, 39.51, 38.07, 37.78, 37.32, 36.98, 36.59, 36.20, 35.78, 34.96, 34.42, 31.90, 31.49, 30.31, 30.14, 29.96, 29.67, 29.33, 29.03, 28.21, 27.99, 27.75, 27.20, 24.28, 23.85, 22.79, 22.66, 22.54, 21.03, 19.29, 18.72, 14.04, 11.85.

4.1.10. Synthesis of target compound NH_2-TPE-PEG-Chol

TPE-PEG-Chol (103.6 mg, 0.09 mmol) and TBTU (34.4 mg, 0.11 mmol) were dissolved in 30 mL of $CHCl_3$, and DIEA (19 μL, 0.12 mmol) was added. Then the *N*-boc-ethylenediamine (14.4 mg, 0.09 mmol) was added to the solution. The mixture was stirred at room temperature for 8 h, then it was evaporated in vacuo. The crude product was purified by column chromatography ($CHCl_2$: MeOH = 20: 1) to afford white solid. Then the white solid was dissolved in 4 mL HCl/1,4-Dioxane and was

stirred at room temperature for 3 h. The reaction was quenched with saturated sodium hydrogen sulfite solution, followed by extraction with ethyl acetate and then the organic layers were dried over Na_2SO_4, filtered, and concentrated. The obtained crude product was purified by silica column chromatography to yield the target compound NH_2-TPE-PEG-Chol (26.1 mg, 29% yield) as white solid. HRMS, ESI^+, *m/z*: calcd for $C_{71}H_{96}N_4O_8$ $(M + H)^+$ 1133.73009, found 1133.72948. ^1H NMR (500 MHz, $CDCl_3$) δ: 7.59–7.52 (4 H, m), 7.08–6.95 (14 H, m), 5.35, 5.33 (1 H, d, $J = 4.5$ Hz), 4.59 (1 H, dd, $J = 11.7$, 8.2 Hz), 3.60 (10 H, d, $J = 12.2$ Hz), 3.56–3.28 (8 H, m), 3.20 (2 H, s), 2.58–2.43 (2 H, m), 2.41 (2 H, dd, $J = 19.9$, 12.8 Hz), 2.30 (2 H, ddd, $J = 22.8$, 15.5, 7.8 Hz), 2.02–1.98 (4 H, m), 1.87–1.82 (4 H, m), 1.71 (2 H, dd, $J = 12.0$, 5.9 Hz), 1.69–1.41 (9 H, m), 1.16–1.05 (4 H, m), 1.00–0.92 (4 H, m), 0.90–0.85 (12 H, m), 0.67 (2 H, d, $J = 4.6$ Hz). ^{13}C NMR (126 MHz, $CDCl_3$) δ: 172.62, 171.66, 171.34, 147.23, 146.56, 146.50, 146.40, 145.46, 142.90, 142.73, 141.41, 141.37, 141.00, 139.82, 139.62, 138.96, 131.45, 131.37, 129.90, 128.17, 127.97, 127.21, 126.90, 126.68, 124.72, 124.44, 124.35, 123.44, 122.81, 119.02, 118.87, 77.58, 77.16, 76.74, 74.50, 70.58, 70.42, 70.17, 70.04, 69.94, 56.89, 56.37, 50.24, 42.51, 39.93, 39.69, 38.82, 38.26, 37.92, 37.16, 36.77, 36.37, 35.94, 32.06, 31.59, 30.63, 30.33, 30.14, 29.66, 29.48, 29.21, 28.16, 27.92, 24.44, 24.02, 22.82, 22.70, 21.21, 19.45, 18.89, 14.23, 12.02.

4.1.11. Synthesis of target compound DiOH-TPE-PEG-Chol

TPE-PEG-Chol (115.9 mg, 0.11 mmol) and TBTU (38.7 mg, 0.12 mmol) were dissolved in 30 mL of $CHCl_3$, and DIEA (21 μL, 0.14 mmol) was added. Then the *N*-(3-aminopropyl) diethanolamine (17.8 μL, 0.11 mmol) was added to the solution. The mixture was stirred at room temperature for 8 h, then it was evaporated in vacuo. The crude product was purified by column chromatography ($CHCl_2$: MeOH = 20: 1) to afford target compound DiOH-TPE-PEG-Chol (26.8 mg, 19.7% yield) as a white solid. HRMS, ESI^+, *m/z*: calcd for $C_{76}H_{106}N_4O_{10}$ $(M + H)^+$ 1235.79817, found 1235.79653. ^1H NMR (500 MHz, $CDCl_3$) δ: 7.55, 7.53 (2 H, d, $J = 8.3$ Hz), 7.36 (4 H, s), 7.13–6.98 (12 H, m), 5.35 (1 H, s), 4.58 (1 H, m), 3.75–3.30 (22 H, m), 2.84 (1 H, d, $J = 16.5$ Hz), 2.63 (2 H, s), 2.33–2.29 (6 H, m), 2.03, 2.02 (6 H, d, $J = 5.7$ Hz), 1.84 (3 H, s), 1.63 (3 H, dt, $J = 18.7$, 15.6 Hz), 1.45 (5 H, dd, $J = 25.3$, 16.1 Hz), 1.16 (5 H, d, $J = 15.6$ Hz), 0.88 (23 H, t, $J = 32.8$ Hz), 0.68 (2 H, s). ^{13}C NMR (126 MHz, $CDCl_3$) δ 176.67, 172.54, 168.33, 167.08, 148.40, 148.37, 146.30, 144.66, 138.16, 130.41, 129.90, 129.10, 128.76, 127.26, 123.65, 123.55, 123.15, 122.65, 118.32, 118.22, 118.08, 114.57, 74.32, 71.36, 70.49, 70.44, 70.27, 70.04, 69.80, 66.91, 55.91, 55.39, 50.05, 42.32, 38.71, 35.40, 34.98, 34.17, 34.06, 33.62, 32.86, 31.10, 30.81, 30.69, 30.62, 29.66, 29.52, 29.40, 29.35, 28.96, 28.87, 28.79, 28.69, 28.64, 28.53, 28.44, 28.33, 28.29, 28.22, 28.14, 27.19, 26.40, 23.98, 23.48, 23.05, 21.99, 21.86, 21.74, 18.50, 17.92, 13.27, 11.06.

4.1.12. Synthesis of target compound Lys-TPE-PEG-Chol

TPE-PEG-Chol (139.2 mg, 0.13 mmol) and TBTU (53.3 mg, 0.17 mmol) were dissolved in 15 mL of $CHCl_3$, and DIEA (27 μL, 0.17 mmol) was added. Then the *N*-Boc-Lys (26.9 mg, 0.15 mmol) was added to the solution. The mixture was stirred at room temperature for 8 h, then it was evaporated in vacuo. The crude product was purified by column chromatography ($CHCl_2$: MeOH = 20: 1) to afford white solid. Then the white solid was dissolved in 2 mL HCl/1,4-Dioxane and was stirred at room temperature for 5 h. The reaction was quenched with saturated sodium hydrogen sulfite solution, followed by extraction with ethyl acetate and then the organic layers were dried over Na_2SO_4, filtered, and concentrated. The obtained crude product was purified by silica column chromatography to yield the target compound Lys-TPE-PEG-Chol (42.7 mg, 27% yield) as white solid. HRMS, ESI^+, *m/z*: calcd for $C_{75}H_{102}N_4O_{10}$ $(M + H)^+$ 1219.76687, found 1219.76941. ^1H NMR (300 MHz, MeOD) δ: 7.56–7.51 (4 H, t, $J = 6.9$ Hz), 7.10 (10 H, d, $J = 13.0$ Hz), 6.96 (4 H, d, $J = 3.6$ Hz), 5.28 (1 H, dd, $J = 9.4$, 4.7 Hz), 4.56–4.41 (1 H, m), 3.59–3.38 (17 H, m), 3.20 (2 H, t, $J = 6.6$ Hz), 2.52 (2 H, t, $J = 5.7$ Hz), 2.42, 2.40 (2 H, d, $J = 5.9$ Hz), 2.26, 2.24 (2 H, d, $J = 7.4$ Hz), 1.96–1.80 (6 H, ddd, $J = 36.7$, 14.2, 9.8 Hz), 1.61–1.43 (7 H, m), 1.37 (7 H, t, $J = 4.2$ Hz), 1.10 (4 H, dd, $J = 18.8$, 10.0 Hz), 0.97–0.89 (4 H, m), 0.88–0.81 (20 H, ddd, $J = 18.0$, 11.1, 4.9 Hz), 0.65 (3 H, d, $J = 7.0$ Hz). ^{13}C NMR (75 MHz, MeOD) δ: 172.17, 171.89, 169.44, 167.66, 167.48, 152.65, 146.26, 146.18, 142.17, 142.11, 140.64, 140.54, 138.98, 131.81, 131.69, 130.53, 130.43, 129.02, 128.75, 128.55, 128.03, 127.24, 127.10, 126.28, 125.95, 124.17, 123.97, 123.43, 123.26, 122.57, 122.39, 121.87, 114.79, 114.45, 73.79, 69.65, 69.37, 69.28, 68.65, 68.22, 67.44, 64.00, 56.15, 55.62, 49.59, 42.64, 41.64, 39.17, 38.82, 38.52, 38.22, 37.32, 36.97, 36.34, 36.14, 35.89, 35.51, 35.14, 31.27, 31.17, 30.55, 30.27, 29.21, 28.87, 28.51, 27.46, 27.23, 26.97, 23.50, 23.10, 22.15, 21.85, 21.62, 21.39, 20.33, 18.22, 17.70, 12.80, 12.39, 10.82.

4.2. The photophysical properties of R-TPE-PEG-Chol

4.2.1. UV–vis absorption spectra

1 mg R-TPE-PEG-Chol were dissolved by DMSO to get 10 μM R-TPE-PEG-Chol solution. Then the max absorption peaks of R-TPE-PEG-Chol were detected by UV spectrophotometer and the absorption peak of DMSO as control.

4.2.2. The fluorescence emission spectrum

1 mg R-TPE-PEG-Chol were dissolved in DMSO to get 300 μM R-TPE-PEG-Chol stock solution. Then, 166 μL stock solution was added into water/DMSO mixture solution with different proportion to afford 10 μM R-TPE-PEG-Chol in different solvents (THF, MeOH, Water and DMSO) and in different proportion water/DMSO mixture solution. The fluorescence emission spectrum of R-TPE-PEG-Chol were investigated using fluorescence spectrophotometer under 330 nm excitation wavelength.

4.2.3. The molar absorption coefficient

1 mg R-TPE-PEG-Chol were dissolved in DMSO to get 300 μM R-TPE-PEG-Chol stock solution. Then, 166 μL stock solution was added into different solvents (THF, MeOH, Water and DMSO) to afford different concentration (0.1 μM, 0.25 μM, 0.5 μM, 1 μM, 2.5 μM, 5 μM, 10 μM) of R-TPE-PEG-Chol. Then the absorption in 330 nm of R-TPE-PEG-Chol were detected by UV spectrophotometer. Taking the absorbance as the ordinate and the concentration as the abscissa to obtain a linear regression equation, and the slope of the straight line is molar absorption coefficient. The molar absorptivity coefficient (ϵ) was calculated by the following formula: $\epsilon = \frac{A}{lc}$ (ϵ: Molar absorption coefficient, *A*: Absorbance at a specific wavelength, *l*: Optical path length, *c*: Per unit volume concentration).

4.2.4. The fluorescence quantum yield and Stokes' shift

1 mg R-TPE-PEG-Chol were dissolved in DMSO to get 300 μM R-TPE-PEG-Chol stock solution. Then, 166 μL stock solution was added into water to get 10 μM R-TPE-PEG-Chol solution and 1 mg quinoline sulfate were dissolved by 0.05 M H_2SO_4 to get 2 μg/mL quinoline sulfate. Then the absorption in 330 nm of R-TPE-PEG-Chol and quinoline sulfate were detected by UV spectrophotometer. The fluorescence emission intensity in 475 nm of R-TPE-PEG-Chol and quinoline sulfate were investigated using fluorescence spectrophotometer under 330 nm excitation wavelength. The Fluorescence quantum yields (Φ) were calculated by the following formula: $\Phi = \Phi_s \frac{I_u}{I_s} \frac{A_s}{A_u}$ (Φ: fluorescence quantum yield of the analytes, Φ_s: fluorescence quantum yield of the reference standard, I_u: Integrated fluorescence intensity of the analytes, I_s: Integrated fluorescence intensity of the reference standard, A_u: Absorption of the analytes, A_s: Absorption of the reference standard. Quantum yield which is determined using quinoline sulfate as the standard). Moreover, the Stokes' shift is calculated by the difference between the maximum of the lowest excitation band and that of the highest emission band.

4.2.5. Aggregate particle size and TEM imaging

50 μL R-TPE-PEG-Chol stock solution (300 μM in DMSO) was added into 4.95 mL water, and the mixture solution was detected using Dynamic light scattering (DLS). An appropriate amount of our designed probes solution was dropped into the copper mesh, then were stained with 0.5% phosphorus tungstate. After drying, the aggregate state of probes in aqueous solution was imaged by transmission electron microscope (TEM), the solution of probes in MeOH was control.

4.3. Detection of activated $CD8^+$T cells by R-TPE-PEG-Chol

4.3.1. Isolation and culturing of $CD8^+$T cells

The animal protocols used in this study were approved by the Animal Ethics Committee of China Pharmaceutical University. Spleens from C57BL/6 mice were ground through a 70-μm filter, and red blood cells were removed by incubation with ACK lysis buffer for 5 min at 4 °C. Then, the splenic cells were centrifuged and isolated by the Easysep Mouse $CD8^+$T cell isolation kit (Stemcell Technologies; catalog no. 19853) to obtain naïve mouse $CD8^+$T cells. Naïve human $CD8^+$T cells were isolated from human peripheral blood mononuclear cells (PBMC) by the Easysep Human $CD8^+$T cell isolation kit (Stemcell Technologies; catalog no. 17953). The human PBMC were obtained from the peripheral blood of healthy donors following an approved the Ethics Committee of Nanjing Jingdu hospital. All the donors had been informed before the experiments.

To activate $CD8^+$T cells, naïve mouse $CD8^+$T cells were resuspended in RPMI 1640 medium containing recombinant mouse IL-2 (10 ng/mL), penicillin, streptomycin, and 10% fetal calf serum (FBS), then cells were cultured in plate pre-coated with anti-CD3 (3 μg/mL) and anti-CD28 (2 μg/mL), and incubated at 37 °C in humidified atmosphere of 5% CO_2. Naïve human $CD8^+$T cells were resuspended in ImmunoCult™ XF T cell expansion medium containing recombinant mouse IL-2 (10 ng/mL), then cells were cultured in plate pre-coated with anti-CD3 (3 μg/mL) and anti-CD28 (2 μg/mL), and incubated at 37 °C in humidified atmosphere of 5% CO_2. Unstimulated T cells were cultured in absence of the activating antibody and IL-2. At the end of the incubation, both naïve and activated T cells were suspended in phosphate buffer saline (PBS) for *in vitro* and *ex vivo* studies.

4.3.2. Cytotoxicity study

CCK8 assays were used to evaluate the cytotoxicity of R-TPE-PEG-Chol on T cells. T cells were seeded in 96-well plates at a density of 1×10^5 cells per well. After culturing overnight, the medium in each well was replaced with 200 μL of fresh medium containing different concentrations of R-TPE-PEG-Chol. 24 h later, 20 μL CCK8 solution was added into each well. After 4 h of incubation, the absorption of each well at 450 nm was recorded via a plate reader (BioTek, Cytation 5). Each trial was performed with 3 wells in parallel.

4.3.3. Screening of optimal incubation time and concentration for imaging the activated $CD8^+$T cells

1×10^6 naïve $CD8^+$T cells were incubated in 1 mL RPIM 1640 medium containing different concentrations (0, 2.5, 4, 10, 20, 50 μM) of R-TPE-PEG-Chol for 10 min and washed twice with ice cold PBS by centrifugation at 1500 rpm for 5 min, and cultured in plate pre-coated with anti-CD3 (3 μg/mL) and anti-CD28 (2 μg/mL) for 24 h. Then, T cells were collected and washed twice with ice cold PBS by centrifugation at 1500 rpm for 5 min. Finally, T cells were resuspended at 1×10^6/mL in ice cold PBS, and the fluorescence of R-TPE-PEG-Chol was investigated using flow cytometry. Additionally, 1×10^6 naïve $CD8^+$T cells were incubated in 1 mL RPIM 1640 medium containing 20 μM R-TPE-PEG-Chol for different time (0, 5, 10, 20, 30, 45 min) and washed twice with ice cold PBS by centrifugation at 1500 rpm for 5 min, and cultured in plate pre-coated with anti-CD3 (3 μg/mL) and anti-CD28 (2 μg/mL) for 24 h. Then, T cells were collected and washed twice with ice cold PBS by centrifugation at 1500 rpm for 5 min. Finally, T cells were resuspended at 1×10^6/mL in ice cold PBS, and the fluorescence of R-TPE-PEG-Chol was investigated using flow cytometry.

4.3.4. Screening of optimal fluorescent probe for imaging the activated $CD8^+$T cells

1×10^6 naïve $CD8^+$T cells were incubated in 1 mL RPIM 1640 medium containing 10 μM OH-TPE-PEG-Chol for 20 min, and 1 mL RPIM 1640 medium containing 20 μM DiOH-TPE-PEG-Chol for 20 min, and 1 mL RPIM 1640 medium containing 20 μM COOH-TPE-PEG-Chol for 30 min, and 1 mL RPIM 1640 medium containing 2.5 μM NH_2-TPE-PEG-Chol for 20 min, and 1 mL RPIM 1640 medium containing 2.5 μM Lys-TPE-PEG-Chol for 10 min, respectively. Anchored naïve T cells were washed twice with ice cold PBS by centrifugation at 1500 rpm for 5 min, and cultured in plate pre-coated with anti-CD3 (3 μg/mL) and anti-CD28 (2 μg/mL) for 24 h. Then, T cells were collected and washed twice with ice cold PBS by centrifugation at 1500 rpm for 5 min. Finally, T cells were resuspended at 1×10^6/mL in ice cold PBS, and the fluorescence of R-TPE-PEG-Chol was investigated using flow cytometry.

4.4. The influence of COOH-TPE-PEG-Chol on the key physiological functions of T cells

4.4.1. The viability analysis

1×10^6 naïve $CD8^+$T cells were incubated in 1 mL RPIM 1640 medium containing 20 μM COOH-TPE-PEG-Chol for 30 min and then washed twice with ice cold PBS by centrifugation at 1500 rpm for 5 min. 1×10^6 naïve $CD8^+$T cells and 1×10^6 naïve COOH-TPE-PEG-Chol anchored $CD8^+$T cells were resuspended in RPMI 1640 medium containing recombinant mouse IL-2 (10 ng/mL), penicillin, streptomycin, and 10% FBS, and cultured in 6-well plate pre-coated with anti-CD3 (3 μg/mL) and anti-CD28 (2 μg/mL). Fresh medium was replaced on day 4 of culture. On day 2, 4 and 7, T cells were harvested for Trypan blue staining (Trypan Blue Staining Cell Viability Assay Kit, C0011, Beyotime Biotechnology), and 20 fields of view were randomly selected in Countstar® BioTech Automated Cell Counter to count the number of viable cells and dead cells. Survival rate (%) = number of viable cells/total number of cells × 100%.

CCK8 assay was also used to assess the effect of COOH-TPE-PEG-Chol on the cell viability of T cells. 1×10^5 naïve $CD8^+$T cells and 1×10^5 naïve COOH-TPE-PEG-Chol anchored $CD8^+$T cells were resuspended in RPMI 1640 medium containing recombinant mouse IL-2 (10 ng/mL), penicillin, streptomycin, and 10% FBS, and cultured in plate pre-coated with anti-CD3 (3 μg/mL) and anti-CD28 (2 μg/mL). On day 2, 4 and 7, CCK8 solution was added into each well. After incubation, the absorption of each well at 450 nm was recorded via a plate reader (BioTek, Cytation 5). Each trial was performed with 3 wells in parallel.

4.4.2. The proliferation assays

1×10^6 naïve $CD8^+$T cells were incubated in 1 mL RPIM 1640 medium containing 20 μM COOH-TPE-PEG-Chol for 30 min and then washed twice with ice cold PBS by centrifugation at 1500 rpm for 5 min. 1×10^6 naïve $CD8^+$T cells and 1×10^6 naïve COOH-TPE-PEG-Chol anchored $CD8^+$T cells were resuspended at RPMI 1640 medium containing recombinant mouse IL-2 (10 ng/mL), penicillin, streptomycin, and 10% FBS, and cultured in plate pre-coated with anti-CD3 (3 μg/mL) and anti-CD28 (2 μg/mL). On day 2, 4 and 7, the cells were collected and counted. Fold expansion rate (%) = Number of cells/Number of cells (day 0) × 100%.

4.4.3. The trans vascular migration analysis

We first established a confluent monolayer endothelial cell model in transwell. Human umbilical vein endothelial cells (HUVECs) were seeded onto the upper chamber of the 24 mm transwell with 3 μm pore and cultured with medium containing 10% FBS. The integrity of the cell monolayer was evaluated by measuring the transepithelial electrical resistance (TEER) values using a Millicell-ERS voltohmeter (Millipore).

Cell monolayers with TEER value higher than 300 Ω/cm^2 were used for the migration studies. 1×10^6 naïve CD8$^+$T cells were incubated in 1 mL RPIM 1640 medium containing 20 μM COOH-TPE-PEG-Chol for 30 min and then washed twice with ice cold PBS by centrifugation at 1500 rpm for 5 min. 1×10^6 naïve CD8$^+$T cells and 1×10^6 naïve COOH-TPE-PEG-Chol anchored CD8$^+$T cells were resuspended in RPMI 1640 medium containing recombinant mouse IL-2 (10 ng/mL), penicillin, streptomycin, and 10% FBS, and cultured in 6-well plate pre-coated with anti-CD3 (3 μg/mL) and anti-CD28 (2 μg/mL). T cells were harvested, and 1×10^6 CD8$^+$T cells or 1×10^6 COOH-TPE-PEG-Chol anchored CD8$^+$T cells were added to the upper chamber with TNFα (25 ng/mL) for 4 h, and monocyte chemotactic protein 1 (MCP-1, 20 ng/mL) was added into the lower chamber. After 12 h of incubation, the number of T cells in the lower chamber was counted.

4.4.4. The chemotaxis analysis

1×10^6 naïve CD8$^+$T cells were incubated in 1 mL RPIM 1640 medium containing 20 μM COOH-TPE-PEG-Chol for 30 min and then washed twice with ice cold PBS by centrifugation at 1500 rpm for 5 min. 1×10^6 naïve CD8$^+$T cells and 1×10^6 naïve COOH-TPE-PEG-Chol anchored CD8$^+$T cells were resuspended in RPMI 1640 medium containing recombinant mouse IL-2 (10 ng/mL), penicillin, streptomycin, and 10% FBS, and cultured in 6-well plate pre-coated with anti-CD3 (3 μg/mL) and anti-CD28 (2 μg/mL). T cells were harvested, and 1×10^6 CD8$^+$T cells or 1×10^6 COOH-TPE-PEG-Chol anchored CD8$^+$T cells were added into the upper chamber of the transwell, and different concentration of MCP-1 (5, 20, and 100 ng/mL) were added into the lower chamber for inducing the migration of T cells. After incubation for 12 h, the cells in the lower chamber were harvested and counted. The chemotaxis index ($(n_{COOH\text{-}TPE\text{-}PEG\text{-}Chol\ anchored\ CD8+T\ cells} - n_{control})/n_{control}$) was calculated, where $n_{COOH\text{-}TPE\text{-}PEG\text{-}Chol\ anchored\ CD8+T\ cells}$ was the counted numbers of COOH-TPE-PEG-Chol anchored CD8$^+$T cells in the lower chamber and $n_{control}$ was the counted numbers of un-anchored CD8$^+$T cells in the lower chamber in the absence of MCP-1.

4.4.5. The activation analysis

1×10^6 naïve CD8$^+$T cells were incubated in 1 mL RPIM 1640 medium containing 20 μM COOH-TPE-PEG-Chol for 30 min and then washed twice with ice cold PBS by centrifugation at 1500 rpm for 5 min. The naïve CD8$^+$T cells and naïve COOH-TPE-PEG-Chol anchored CD8$^+$T cells were cultured in plate pre-coated with anti-CD3 (3 μg/mL) and anti-CD28 (2 μg/mL) agonist antibodies. After 24 h of culture, T cells were collected and washed twice with ice cold PBS by centrifugation at 1500 rpm for 5 min. Then, T cells were resuspended at 1×10^7/mL in ice cold PBS, and stained with FITC anti-mouse CD69 antibody (1 μg/mL, BioLegend) for 20 min at 4 °C. Finally, T cells were washed twice with ice cold PBS by centrifugation at 1500 rpm for 5 min and resuspended at 1×10^6/mL in ice cold PBS. The fluorescence of CD69 was detected by flow cytometry.

To assess the influence of COOH-TPE-PEG-Chol on activation signaling of CD8$^+$T cells, 1×10^6 naïve CD8$^+$T cells were incubated in 1 mL RPIM 1640 medium containing 20 μM COOH-TPE-PEG-Chol for 30 min and then washed twice with ice cold PBS by centrifugation at 1500 rpm for 5 min. The naïve CD8$^+$T cells and naïve COOH-TPE-PEG-Chol anchored CD8$^+$T cells were cultured in plate pre-coated with anti-CD3 (3 μg/mL) and anti-CD28 (2 μg/mL) agonist antibodies. After 24 h of culture, T cells were collected and washed twice with ice cold PBS by centrifugation at 1500 rpm for 5 min. The whole-cell protein extracts were isolated using radioimmunoprecipitation assay lysis buffer. Protein concentration was determined by the BCA Protein Assay Kit (Keygen Biotech). About 30 μg of total protein was loaded, fractionated by SDS-polyacrylamide gel electrophoresis, transferred to polyvinylidene difluoride membrane, and probed with anti-β-actin (Absin), anti-pCD3ζ (Tyr142) (Thermo Fisher Scientific) and anti-pZAP70 (Tyr319) (Cell Signaling Technology). Signal was detected using a chemiluminescence imaging system (Tanon).

4.4.6. The cytokines secretion analysis

1×10^6 naïve CD8$^+$T cells were incubated in 1 mL RPIM 1640 medium containing 20 μM COOH-TPE-PEG-Chol for 30 min and then washed twice with ice cold PBS by centrifugation at 1500 rpm for 5 min. The naïve CD8$^+$T cells and naïve COOH-TPE-PEG-Chol anchored CD8$^+$T cells were stimulated with anti-CD3 (3 μg/mL) and anti-CD28 (2 μg/mL) agonist antibodies. After 24 h of culture, T cells were collected and washed twice with ice cold PBS by centrifugation at 1500 rpm for 5 min. Then, T cells were resuspended at 1×10^7/mL in ice cold PBS, and stained with FITC anti-mouse GzmB (1 μg/mL, BioLegend), APC anti-mouse IFNγ (0.6 μg/mL, BioLegend) and PE anti-mouse TNFα (0.5 μg/mL, BioLegend) for 20 min at 4 °C. Finally, T cells were washed twice with ice cold PBS by centrifugation at 1500 rpm for 5 min and resuspended at 1×10^6/mL in ice cold PBS. The fluorescence of GzmB, IFNγ and TNFα were detected by flow cytometry.

4.5. The efficiency of COOH-TPE-PEG-Chol for real-time monitoring T cells with heterogeneous activation levels

4.5.1. Confocal imaging of the cholesterol distribution on naïve and activated T cells membrane

The naïve and activated T cells were collected, and fixed with 4% Paraformaldehyde (PFA) for 15 min at room temperature. Then, cells were washed twice with PBS and stained with Filipin III (50 μg/mL) for 30 min at 4 °C, and plated in confocal chambers after centrifugation. Images were collected using a Zeiss LSM 880 confocal microscope and analyzed using Zeiss ZEN software.

4.5.2. Real-time monitoring the activation of T cells by COOH-TPE-PEG-Chol

The naïve T cells were incubated in 1 mL RPIM 1640 medium containing 20 μM COOH-TPE-PEG-Chol for 30 min at 37 °C, and cultured in plate pre-coated with anti-CD3 (3 μg/mL) and anti-CD28 (2 μg/mL) for 24 h. Then naïve T cells and activated T cells were collected respectively and stained with Alexa Fluor 647 anti-mouse TCR antibody for 15 min at 4 °C. T cells were fixed with 4% PFA for 15 min at room temperature, and collected and washed with PBS, and plated in confocal chambers. Images were collected using a Zeiss LSM 880 confocal microscope and analyzed using Zeiss ZEN software. Fluorescence was analyzed with ImageJ, and the signal-to-noise ratio was calculated as the ratio of probe fluorescence in the TCR nanocluster to probe fluorescence in the non-TCR nanocluster region, and the signal-to-background ratio was calculated as the ratio of probe fluorescence in the TCR nanocluster to the fluorescence in the background without probe.

To verify the colocalization of COOH-TPE-PEG-Chol and TCR nanoclusters, images of COOH-TPE-PEG-Chol fluorescence and TCR fluorescence on activated T cells were collected using a Zeiss LSM 880 confocal microscope. Images were imported into the Fiji/ImageJ software, which contains a number of pre-installed plugins including a procedure for colocalization analysis. The co-localization of COOH-TPE-PEG-Chol and TCR, and 2D intensity histograms, Pearson coefficients were exported with Fiji/ImageJ.

The naïve T cells were incubated in 1 mL RPIM 1640 medium containing 20 μM COOH-TPE-PEG-Chol for 30 min at 37 °C, and cultured in plate pre-coated with anti-CD3 (3 μg/mL) and anti-CD28 (2 μg/mL) for different time (0, 6, 12, 24 h). Then, the cells were collected and washed twice with ice cold PBS by centrifugation at 1500 rpm for 5 min. Finally, T cells were resuspended at 1×10^6/mL in ice cold PBS, the fluorescence intensity of COOH-TPE-PEG-Chol was investigated using flow cytometry.

4.5.3. The lifetime of COOH-TPE-PEG-Chol on the cell-surface

1×10^6 naïve CD8$^+$T cells were incubated in 1 mL RPIM 1640 medium containing 20 μM COOH-TPE-PEG-Chol for 30 min at 37 °C, and CD8$^+$T cells were collected and washed twice with PBS. The COOH-TPE-PEG-Chol anchored naïve CD8$^+$T cells were cultured in plate pre-coated

against anti-CD3 (3 μg/mL) and anti-CD28 (2 μg/mL) for 24 h, and then the COOH-TPE-PEG-Chol anchored activated $CD8^+$T cells were collected and used to detect the lifetime of COOH-TPE-PEG-Chol. The COOH-TPE-PEG-Chol anchored activated $CD8^+$T cells were reactivated by anti-CD3 (3 μg/mL) and anti-CD28 (2 μg/mL) for 30 min at different time (0, 6, 12, 24, 48, 72, 96 h). T cells were collected and washed twice with ice cold PBS by centrifugation at 1500 rpm for 5 min. Then, T cells were stained with 5 μM SYTO 82 orange dye for 10 min. The fluorescence of COOH-TPE-PEG-Chol was detected by LSM 880 confocal microscope and flow cytometry.

4.5.4. Real-time monitoring the activation of human $CD8^+$T cells by COOH-TPE-PEG-Chol

The naïve T cells were incubated in 1 mL RPIM 1640 medium containing 20 μM COOH-TPE-PEG-Chol for 30 min at 37 °C, and T cells were collected and washed twice with PBS. T cells were resuspended at ImmunoCult™ XF T cell expansion medium containing, and cultured in plate pre-coated against anti-CD3 with different concentration (0, 0.185, 0.375, 0.75, 1.5, 3 μg/mL) or anti-CD3 (3 μg/mL) plus anti-CD28 (2 μg/mL) for 24 h. T cells were collected and washed twice with ice cold PBS by centrifugation at 1500 rpm for 5 min. Then, T cells were stained with 5 μM SYTO 82 orange dye for 10 min, and plated in confocal chambers. Images were collected using a Zeiss LSM 880 confocal microscope and analyzed using Zeiss ZEN software. Moreover, the above T cells were resuspended at 1×10^6/mL in ice cold PBS and further analyzed for the fluorescence intensity of COOH-TPE-PEG-Chol by flow cytometry.

The naïve T cells were incubated in 1 mL RPIM 1640 medium containing 20 μM COOH-TPE-PEG-Chol for 30 min at 37 °C, and T cells were collected and washed twice with PBS. T cells were cultured in plate pre-coated against anti-CD3 (3 μg/mL) and anti-CD28 (2 μg/mL) for 24 h, and then T cells were collected. A surgically resected human ovarian cancer tissue was obtained from a female ovarian cancer patient following an approved the Ethics Committee of Nanjing Jingdu hospital. The COOH-TPE-PEG-Chol anchored activated $CD8^+$T cells were injected into the ovarian cancer tissue, and incubated at 37 °C, 5% CO_2 under medium for different time (0, 4, 8, 16, 24, 48 h). At the end of different time point, the cancer tissues were collected and stored at −80 °C for further research. Frozen cancer tissues were sectioned and fixed for fluorescent immunohistochemistry staining. Frozen tissue sections were permeabilized using 0.3% Triton X-100, and stained with rabbit anti-human pZAP70 (phosphor Y292, Abcam) for 1 h at room temperature, and then stained with Alexa Fluor 594-conjugated goat anti-rabbit lgG (2 μg/mL, Invitrogen) for 1 h at room temperature. Meanwhile, sections were also stained with APC anti-human CD8a antibody (1 μg/mL, Biolegend) for 1 h at room temperature and 5 μM SYTO 82 orange dye for 10 min. Finally, these sections were sealed after washed with PBS, and observed using LSM 880 confocal microscope.

4.6. Statistical analysis

All the data were presented as mean ± SEM. Student's *t*-test was used for a comparison between two groups, and the differences among multiple groups were analyzed by one-way ANOVA. 95% confidence intervals (CI) were calculated by Student's *t*-test or one-way ANOVA. Statistical significance was set at $^*P < 0.05$, $^{**}P < 0.01$, $^{***}P < 0.001$, $^{****}P < 0.0001$ and n.s denotes no significant difference. (GraphPad Prism 8.0.1).

Author contributions

K.M.L. conducted cell experiments and wrote the manuscript. Y.C. conducted the synthesis experiments. N.C.Z. assisted in cell experiments. S.J.C. assisted in frozen tissue sections. M.J. and L.J.X. assisted in analysis the data. M.X.H. designed all experiments, supervised the cell experiments and wrote the manuscript. C.Z. conceived the project and supervised all experiments.

Declaration of competing interest

The authors declare that they have no known competing financial interests or personal relationships that could have appeared to influence the work reported in this paper.

Data availability

Data will be made available on request.

Acknowledgments

This work was supported by the National Natural Science Foundation of China (92159304, 82130102, 81930099, 81773664, 82104102), the Natural Science Foundation of Jiangsu Province (BK20212011), Technology innovation project of Nucleic acid drug from National Center of Technology Innovation for Biopharmaceuticals (NCTIB2022HS01014), "Double First-Class" University project (CPU2022QZ05), 111 Project from the Ministry of Education of China and the State Administration of Foreign Expert Affairs of China (No. 111-2-07, B17047), and the Project Program of State Key Laboratory of Natural Medicines (China Pharmaceutical University, No. SKLNMZZ202223).

Appendix A. Supplementary data

Supplementary data to this article can be found online at https://doi.org/10.1016/j.ejmech.2022.115073.

References

[1] B.V. Kumar, T.J. Connors, D.L. Farber, Human T cell development, localization, and function throughout life, Immunity 48 (2018) 202–213.
[2] R.J. Brownlie, R. Zamoyska, T cell receptor signalling networks: branched, diversified and bounded, Nat. Rev. Immunol. 13 (2013) 257–269.
[3] A.J. Walsh, K.P. Mueller, K. Tweed, I. Jones, C.M. Walsh, N.J. Piscopo, N.M. Niemi, D.J. Pagliarini, K. Saha, M.C. Skala, Classification of T-cell activation via autofluorescence lifetime imaging, Nat. Biomed. Eng. 5 (2021) 77–88.
[4] A.M. van der Leun, D.S. Thommen, T.N. Schumacher, CD8(+) T cell states in human cancer: insights from single-cell analysis, Nat. Rev. Cancer 20 (2020) 218–232.
[5] M.A. Stanczak, S.S. Siddiqui, M.P. Trefny, D.S. Thommen, K.F. Boligan, S. von Gunten, A. Tzankov, L. Tietze, D. Lardinois, V. Heinzelmann-Schwarz, M. von Bergwelt-Baildon, W. Zhang, H.J. Lenz, Y.H. Han, C.I. Amos, M. Syedbasha, A. Egli, F. Stenner, D.E. Speiser, A. Varki, A. Zippelius, H. Laubli, Self-associated molecular patterns mediate cancer immune evasion by engaging Siglecs on T cells, J. Clin. Invest. 128 (2018) 4912–4923.
[6] L.E. Holz, V. Benseler, M. Vo, C. McGuffog, N. Van Rooijen, G.W. McCaughan, D. G. Bowen, P. Bertolino, Naive CD8 T cell activation by liver bone marrow-derived cells leads to a "neglected" IL-2 low Bimhigh phenotype, poor CTL function and cell death, J. Hepatol. 57 (2012) 830–836.
[7] L. Yu, F. Yang, F. Zhang, D. Guo, L. Li, X. Wang, T. Liang, J. Wang, Z. Cai, H. Jin, CD69 enhances immunosuppressive function of regulatory T-cells and attenuates colitis by prompting IL-10 production, Cell Death Dis. 9 (2018) 905.
[8] P.L. Choyke, Can molecular imaging measure T-cell activation? Cancer Res. 80 (2020) 2975–2976.
[9] D.R. Soond, E. Bjorgo, K. Moltu, V.Q. Dale, D.T. Patton, K.M. Torgersen, F. Galleway, B. Twomey, J. Clark, J.S. Gaston, K. Tasken, P. Bunyard, K. Okkenhaug, PI3K p110delta regulates T-cell cytokine production during primary and secondary immune responses in mice and humans, Blood 115 (2010) 2203–2213.
[10] J.E. Smith-Garvin, G.A. Koretzky, M.S. Jordan, T cell activation, Annu. Rev. Immunol. 27 (2009) 591–619.
[11] M.X. Hao, S.Y. Hou, W.S. Li, K.M. Li, L.J. Xue, Q.F. Hu, L.L. Zhu, Y. Chen, H.B. Sun, C.Y. Ju, C. Zhang, Combination of metabolic intervention and T cell therapy enhances solid tumor immunotherapy, Sci. Transl. Med. 12 (2020), eaaz6667.
[12] N. Guan, J. Deng, T. Li, X. Xu, J.T. Irelan, M.W. Wang, Label-free monitoring of T cell activation by the impedance-based xCELLigence system, Mol. Biosyst. 9 (2013) 1035–1043.
[13] A.C. Karlsson, J.N. Martin, S.R. Younger, B.M. Bredt, L. Epling, R. Ronquillo, A. Varma, S.G. Deeks, J.M. McCune, D.F. Nixon, E. Sinclair, Comparison of the ELISPOT and cytokine flow cytometry assays for the enumeration of antigen-specific T cells, J. Immunol. Methods 283 (2003) 141–153.
[14] A. Salles, C. Billaudeau, A. Serge, A.M. Bernard, M.C. Phelipot, N. Bertaux, M. Fallet, P. Grenot, D. Marguet, H.T. He, Y. Hamon, Barcoding T cell calcium response diversity with methods for automated and accurate analysis of cell signals (MAAACS), PLoS Comput. Biol. 9 (2013), e1003245.

[15] A.K. Chakraborty, A. Weiss, Insights into the initiation of TCR signaling, Nat. Immunol. 15 (2014) 798–807.
[16] X.L. Su, J.A. Ditlev, E.F. Hui, W.M. Xing, S. Banjade, J. Okrut, D.S. King, J. Taunton, M.K. Rosen, R.D. Vale, Phase separation of signaling molecules promotes T cell receptor signal transduction, Science 352 (2016) 595–599.
[17] S.V. Pageon, T. Tabarin, Y. Yamamoto, Y.Q. Ma, J.S. Bridgeman, A. Cohnen, C. Benzing, Y.J. Gao, M.D. Crowther, K. Tungatt, G. Dolton, A.K. Sewell, D.A. Price, O. Acuto, R.G. Parton, J.J. Gooding, J. Rossy, J. Rossjohn, K. Gaus, Functional role of T-cell receptor nanoclusters in signal initiation and antigen discrimination, P Natl. Acad. Sci. USA 113 (2016) E5454–E5463.
[18] A. Grakoui, S.K. Bromley, C. Sumen, M.M. Davis, A.S. Shaw, P.M. Allen, M. L. Dustin, The immunological synapse: a molecular machine controlling T cell activation, Science 285 (1999) 221–227.
[19] W. Yang, Y. Bai, Y. Xiong, J. Zhang, S. Chen, X. Zheng, X. Meng, L. Li, J. Wang, C. Xu, C. Yan, L. Wang, C.C. Chang, T.Y. Chang, T. Zhang, P. Zhou, B.L. Song, W. Liu, S.C. Sun, X. Liu, B.L. Li, C. Xu, Potentiating the antitumour response of CD8 (+) T cells by modulating cholesterol metabolism, Nature 531 (2016) 651–655.
[20] E. Sezgin, I. Levental, S. Mayor, C. Eggeling, The mystery of membrane organization: composition, regulation and roles of lipid rafts, Nat. Rev. Mol. Cell Biol. 18 (2017) 361–374.
[21] G. Gimpl, K. Gehrig-Burger, Probes for studying cholesterol binding and cell biology, Steroids 76 (2011) 216–231.
[22] X.F. Ma, R. Sun, J.H. Cheng, J.Y. Liu, F. Gou, H.F. Xiang, X.G. Zhou, Fluorescence aggregation-caused quenching versus aggregation-induced emission: a visual teaching technology for undergraduate chemistry students, J Chem. Educ. 93 (2016) 345–350.
[23] D. Wang, B.Z. Tang, Aggregation-induced emission luminogens for activity-based sensing, Accounts Chem. Res. 52 (2019) 2559–2570.
[24] Y.N. Hong, J.W.Y. Lam, B.Z. Tang, Aggregation-induced emission: phenomenon, mechanism and applications, Chem. Commun. (2009) 4332–4353.
[25] Y.N. Hong, J.W.Y. Lam, B.Z. Tang, Aggregation-induced emission, Chem. Soc. Rev. 40 (2011) 5361–5388.
[26] D. Lingwood, K. Simons, Lipid rafts as a membrane-organizing principle, Science 327 (2010) 46–50.
[27] B. Schafer, E. Orban, A. Borics, K. Huszar, A. Nyeste, E. Welker, C. Tomboly, Preparation of semisynthetic lipoproteins with fluorescent cholesterol anchor and their introduction to the cell membrane with minimal disruption of the membrane, Bioconjugate Chem. 24 (2013) 1684–1697.
[28] H. Yao, Q. Zhou, J. Wang, Y.Y. Chen, X.T. Kan, T.B. Wei, Y.M. Zhang, Q. Lin, Highly selective Fe(3+) and F(-)/H2PO4(-) sensor based on a water-soluble cationic pillar[5]arene with aggregation-induced emission characteristic, Spectrochim. Acta Mol. Biomol. Spectrosc. 221 (2019), 117215.
[29] T. Zech, C.S. Ejsing, K. Gaus, B. de Wet, A. Shevchenko, K. Simons, T. Harder, Accumulation of raft lipids in T-cell plasma membrane domains engaged in TCR signalling, EMBO J. 28 (2009) 466–476.
[30] H. Dong, G. Zhu, K. Tamada, L. Chen, B7-H1, a third member of the B7 family, co-stimulates T-cell proliferation and interleukin-10 secretion, Nat. Med. 5 (1999) 1365–1369.
[31] A.J. Michielsen, A.E. Hogan, J. Marry, M. Tosetto, F. Cox, J.M. Hyland, K. D. Sheahan, D.P. O'Donoghue, H.E. Mulcahy, E.J. Ryan, J.N. O'Sullivan, Tumour tissue microenvironment can inhibit dendritic cell maturation in colorectal cancer, PLoS One 6 (2011), e27944.
[32] T.T. Wang, Y.L. Zhao, L.S. Peng, N. Chen, W.S. Chen, Y.P. Lv, F.Y. Mao, J.Y. Zhang, P. Cheng, Y.S. Teng, X.L. Fu, P.W. Yu, G. Guo, P. Luo, Y. Zhuang, Q.M. Zou, Tumour-activated neutrophils in gastric cancer foster immune suppression and disease progression through GM-CSF-PD-L1 pathway, Gut 66 (2017) 1900–1911.
[33] J. Hong, S.L. Fu, Z.Y. Shen, P.H. Lu, K.Y. Chou, Trichosanthin inhibits T cell activation by interfering with the recruitment of ZAP-70 to CD3 zeta chain, Cell Res. 8 (1998) 33–39.
[34] J.T. Chang, E.J. Wherry, A.W. Goldrath, Molecular regulation of effector and memory T cell differentiation, Nat. Immunol. 15 (2014) 1104–1115.
[35] L. Labanieh, R.G. Majzner, C.L. Mackall, Programming CAR-T cells to kill cancer, Nat. Biomed. Eng. 2 (2018) 377–391.